Airborne Sampling of Smoke Emissions

NEWFOUNDLAND NOBE

OFFSHORE BURN EXPERIMENT

SPONSORS:

Environment Canada

U.S. Minerals Management Service

Canadian Coast Guard

Marine Spill Response Corporation

United States Coast Guard

American Petroleum Institute

U.S. Environmental Protection Agency

3-M Ceramics Division

Alaska Clean Seas

Canadian Association of Petroleum Producers

Amoco Production

PERD - Program for Energy Research and Development

Imperial Oil Limited

Hibernia Development

Exxon Biomedical Services

Canmar/Amoco Canada

East Coast Response Incorporated

Beaufort Sea Co-op

Canadian Petroleum Products Institute

Airborne Sampling of Smoke Emissions

Prepared by:

Ronald J. Ferek, John L. Ross, and Peter V. Hobbs
Cloud and Aerosol Research Group
Department of Atmospheric Sciences
University of Washington
Seattle, Washington 98195

for:

Emergencies Science Division
Environmental Technology Centre

Environment Canada Environnement Canada

Minerals Management Service
U.S. Department of the Interior

Citation:

Ferek, R.J., J.L. Ross, and P.V. Hobbs, "Airborne Sampling of Smoke Emissions", Newfoundland Offshore Burn Experiment (NOBE) Report, Emergencies Science Division, Environmental Technology Centre, Environment Canada, Ottawa, Ontario, 56 p., 1997.

Published in May 1997

En40-487/1-1997E
ISBN 0-662-25794-4

Printed in Canada

Reader's Comments

Requests for information, scientific reports, and publications on the Newfoundland Offshore Burn Experiment (NOBE) should be directed to:

Merv Fingas
Emergencies Science Division
Environmental Technology Centre
3439 River Road South
Ottawa, Ontario
K1A 0H3

Review Notice

This report has been reviewed by the Emergencies Science Division of Environment Canada and approved for publication. Approval does not necessarily signify that the contents reflect the views and policies of Environment Canada. Mention of trade names or commercial products does not constitute recommendations or endorsement for use.

TABLE OF CONTENTS

Final Report from University of Washington to Environment Canada for Contract KA168-3-1069/01-SS "Airborne Sampling of Smoke Emissions from the Controlled Burn of 20,000 Gallons of Crude Oil During Open Ocean Conditions Off Newfoundland"

Ronald J. Ferek, John L. Ross and Peter V. Hobbs
Cloud and Aerosol Research Group, Department of Atmospheric Sciences,
University of Washington, Seattle, Washington 98195

SUMMARY

The University of Washington's Cloud and Aerosol Research (CAR) Group utilized its Convair C-131A instrumented research aircraft to obtain measurements of the smoke emissions from the Newfoundland Offshore Burn Experiment (NOBE) on 12 August 1993. A variety of techniques were employed to measure the chemical and physical properties of the gases and particles emitted by the two burns. The objectives were to measure the concentrations of the major combustion products in the smoke plumes, to determine the emission factors (grams of pollutant emitted per kilogram of fuel burned) for a variety of species, to measure the total fluxes of emissions for comparison with the known release rate of the fuel, and to use airborne lidar measurements to characterize the distributions and mass concentration of smoke particles in the plumes.

The major findings of this study are:

- Following ignition, the plumes from the two NOBE burns rose quickly above the marine boundary layer and remained above the surface for at least 40 km downwind (and likely for a much greater distances).

- Smoke concentrations in the plumes diluted rapidly. Total particle mass concentrations were over 1000 $\mu g\ m^{-3}$ near the fires, and 150 $\mu g\ m^{-3}$ between 8 and 16 km downwind of the fires (at plume level, 500 m MSL).

- Airborne lidar measurements of plume cross-sections at several distances downwind, and along the length of the plumes, revealed a high degree of spatial variability in smoke concentrations. Contours of mass concentrations derived from the lidar measurements agreed well with the airborne *in situ* measurements taken during aircraft penetrations of the plumes.

- Emission factors were derived by the carbon balance method for the major combustion products of the fire. The emission factor for particles with diameters $< 3.5\ \mu m$ was measured to be ~87 $g\ kg^{-1}$. This is in reasonable agreement with the smoke yields derived from measurements aboard the NIST blimp, and with our measurements from oil pool fires in Kuwait. The emission factors allow comparison with other sources of pollution; *in situ* burning of oil on the ocean produces emissions comparable to, or lower than, many common sources of air pollution.

- The smoke particles were composed of ~76% elemental carbon (soot), ~8% organic carbon, and 16% was unidentified.

- Fluxes of CO_2 calculated from *in situ* measurements of plume cross-sections were used to estimate the average burn rate of the oil. The burn rate derived in this way agreed with the measured release rate of the oil to within ~ 30%.

1. BACKGROUND

A potentially promising method for removing oil from the ocean is controlled *in situ* burning[1,2]. The most attractive aspect of *in situ* burning is that is can remove large quantities of oil relatively quickly and cheaply[3]. One of the biggest potential drawbacks is air pollution.

In common with any hydrocarbon fuel, the primary combustion products of crude oil are CO_2 and water. In addition, a dense black smoke plume, composed primarily of elemental carbon (soot), is produced. The smoke particles may contain or be coated with condensed organic compounds, sulfates, or liquid water. Other gaseous pollutants produced by the burning of oil are CO, NO_x , SO_2, and a wide range of organic compounds. Of particular concern are polycyclic aromatic hydrocarbons (PAHs), since they are toxic. Many other volatile organic compounds (VOCs) are found in the vapor phase in the smoke, but usually at lower concentrations than those measured above evaporating (non-burning) oil spills. Secondary pollutants (such as O_3) may also be produced by chemical reactions within the smoke plume.

Health concerns arise due to the potentially high concentrations of respirable particles and toxic gases from the burning of oil. For example, PAHs are carcinogenic[4,5]. Laboratory studies[6] of oil burning indicate that the combustion may consume some of the PAHs, but it may also produce some of the more toxic, higher molecular weight species. The nature and concentrations of PAHs from oil fires burning under realistic field conditions was one of the primary interests of the NOBE.

Smoke produced by the *in situ* burning of crude oil will also affect atmospheric visibility. In addition, since smoke generally contains high concentrations of cloud condensation nuclei (CCN), it may affect the microstructure, and therefore the radiative properties, of clouds with which it interacts[7,8]. The effectiveness of elemental carbon particles to act as CCN is probably initially low[9], making them somewhat resistant to

scavenging by clouds and precipitation. However, as the smoke ages, the soot may become coated with materials that enhance its cloud nucleation activity.

Lidar has been used since 1963 to measure the presence of atmospheric aerosols[10]. Not long after, lidar was used to study the smoke from power plants[11,12]. The potential for deriving quantitative information from lidar measurements was demonstrated by Johnson and Uthe[13]. More recently lidar has been used to study arctic hazes[14] and forest fires[15]. As part of the NOBE, we used an airborne lidar to measure the optical properties of the smoke from the *in situ* burning of oil on the ocean, to derive the mass concentrations and fluxes of smoke, and to map the vertical and horizontal extent of the smoke plumes.

2. EXPERIMENTAL

2.1 *Sampling and Instrumentation*

All measurements in the smoke from the two NOBE burns reported here were obtained aboard the University of Washington's (UW) Convair C–131A research aircraft. Most of the time the aircraft flew back and forth across the width of the smoke plume at various distances downwind. Several passes above and below the smoke were also made (above for lidar images, below to sample any smoke near the surface). During each pass through the smoke a 2.5 m^3 polyethylene 'grab' bag aboard the aircraft was filled rapidly with air containing the smoke. This allowed essentially point sampling of the smoke at various locations. Subsequently, various filters and canisters aboard the aircraft were drawn from the grab bag for later chemical analysis. A few times the aircraft flew downwind along the lengths of the smoke plumes, both above and in the smoke, from ~1.5 to ~30 km from the fires.

Particle size distributions in the smoke and in the ambient air were measured continuously by two instruments mounted beneath the wing of the aircraft: a Particle

Measuring Systems (PMS) PCASP-100X, which sizes particles with diameters from 0.1–3.0 μm, and a PMS FSSP-100 probe that measures particles from 2.0–50 μm diameter.

Measurements of the aerosol light extinction coefficient at a wavelength of 0.538 μm were provided by a 6.4 m long optical extinction cell aboard the aircraft that was fed continuously by a ram air inlet. Measurements of the attenuation of a light beam by the smoke in the cell provide the extinction coefficient. Concurrent measurements with an integrating nephelometer provided the light scattering coefficient of the smoke. Subtraction of the light scattering coefficient from the light extinction coefficient yields the light absorption coefficient[16–18].

Atmospheric trace gases that are ubiquitous and exist in relatively high concentrations, such as CO_2, CO, and water vapor, were measured continuously aboard the aircraft. Trace species, such as PAHs and volatile organic compounds (VOCs), were collected on polyurethane filters (PUF) and in stainless steel canisters (SUMMA) for post-flight analysis. A key measurement in the determination of smoke emission factors is the excess (i.e., above ambient) concentration of CO_2 in the plume. To determine this we measured CO_2 with a Li-Cor Model 6262 CO_2 analyzer, which operates on the principle of differential infrared (IR) absorption. Differential IR absorption was also used to measure the absolute humidity of the air, using an Ophir Model IR-2000. Both of these instruments have relatively fast response times, typically <1 s.

The mass concentrations of particles in the plumes were determined by pumping a known volume of smoke from the grab bag through Teflon filters and measuring their changes in weight. Pairs of filters were used; one filter in each pair was preceded by a cyclone separator that allowed only particles <3.5 μm diameter to reach the filter (PM 3.5), and the other filter was preceded by a single impaction stage that removed particles >10 μm diameter (PM 10). Subsequent tests of the inlet to the filters showed that it was relatively inefficient for particles greater than 5 μm. Therefore, the PM 10 results are not accurate

and we will confine our analysis to the sub-3.5 μm fraction, where most of the mass and almost all of the number concentration of the smoke particles reside.

The concentrations of elemental and organic carbon in the aerosol particles were determined on quartz filters, through which smoke from the grab bag had been pumped, and analyzed using a thermal-optical technique[19].

The lidar aboard the C-131A aircraft utilizes a downward pointing Neodymium-Yttrium Aluminum Garnet (Nd-YAG) laser. It is frequency doubled to operate simultaneously at wavelengths of 0.532 and 1.064 μm. The pulse repetition rate is 10 Hz, and the pulse duration is 10 ns. The receiver is a 14" Cassagranian reflector telescope. The outgoing laser beam is routed to the center of the telescope so that the transmitter and receiver are coaxial. The detector for the visible wavelength channel is a photomultiplier tube, and for the IR channel a silicon avalanche photodiode. Data from both channels first passes through a linear pre-amplifier and then the signal is compressed by a logarithmic amplifier. This signal is digitized at a rate of 20 MHz and recorded on Exabyte tape. Only data from the green (λ=0.532 μm) channel will be discussed in this report. The digitization rate gives a vertical resolution of 7.5 m. The pulse repetition rate of 10 Hz could yield a horizontal resolution of ~8 m, depending on the speed of the aircraft. However, in most cases 0.5–1 s averages were used to compensate for the effects of laser inhomogeneities and any non-uniformities in the sea surface from which the laser beam was reflected. This results in horizontal resolution of 40–80 m. Details of the lidar data analysis procedures are given below.

2.2 *Derivation of Optical Depths of the Smoke Plume from Lidar Measurements*

When a pulse from the laser beam hits the ocean surface it produces a very bright reflection. However, if the beam has passed through an intervening smoke layer the strength of the reflection is reduced. If, after passing through clear air (Figure 1a), the

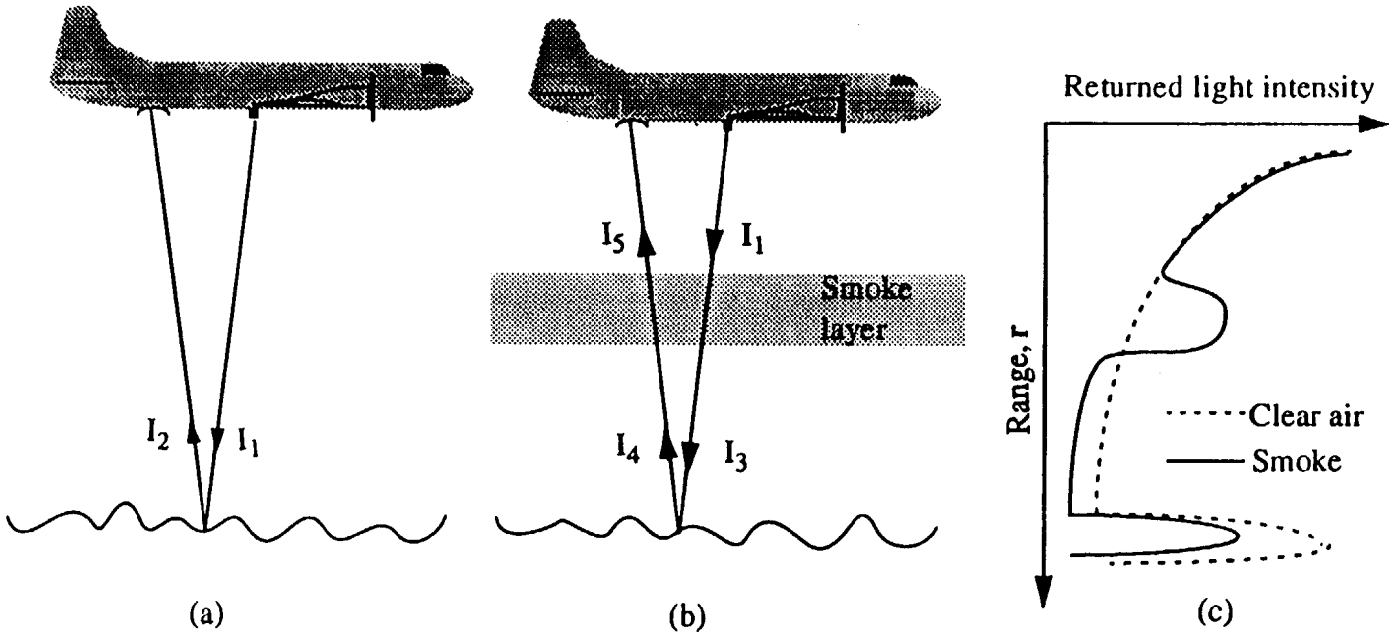

Figure 1. Schematic illustrating the technique for the determination of the optical depth of the smoke from airborne lidar measurements (see text for details).

intensity of the beam incident on the water is I_1, and the intensity of its reflected beam is I_2, the reflection coefficient R of the water is

$$R = \frac{I_2}{I_1} \tag{1}$$

If the laser beam passes through an intervening smoke layer with optical depth δ_i (where the subscript *i* designates a quantity associated with a specific averaged laser shot, typically a 1 s average), and I_1 and I_3 are the intensities of the beam incident on top of the smoke and emerging from the base of the smoke, respectively (Figure 1b)

$$I_3 = I_1 \exp(-\delta_i) \tag{2}$$

Also, from Figure 1b,

$$R = \frac{I_4}{I_3} \tag{3}$$

and,

$$I_5 = I_4 \exp(-\delta_i) \tag{4}$$

Hence, from (1)-(4),

$$\exp(-2\delta_i) = \frac{I_5}{I_2} \tag{5}$$

Figure 1c shows in schematic form the profiles of the returned light intensity for two different laser pulses. The profile through clear air falls off inversely as the square of the range (*r*), but the profile contains a large spike where the lidar beam hits the ocean. The profile through the smoke layer also has a spike in the returned light intensity at the ocean surface, however, it is reduced due to attenuation of the beam. The magnitudes of the two spikes determines the ratio I_5/I_2 and hence δ_i from Eqn. (5).

2.3 *Derivation of Attenuated Backscatter Coefficient from Lidar Measurements*

The attenuated backscatter coefficient of the smoke at range r was determined by comparing the intensity of the returned lidar beam to that at the same range from clear air. The difference between the returned intensities for the two sample profiles shown in Figure 1c is proportional to the ratio of the backscatter coefficients in the clear and smoky air. The vertical distribution of the backscatter coefficient for clear air was determined from the airborne *in situ* measurements of the total light-scattering coefficient. The ratio of backscattering to total scattering in the Rayleigh region is $3/8\pi$, and the backscatter-to-total scattering ratio for the ambient aerosol was assumed to be 0.035[20,21]. The backscatter coefficient for the background (calibration) air was 1.74×10^{-6} m^{-1} str^{-1}. For each laser pulse through the smoke, the attenuated backscatter coefficient at range r, $\beta'(r)_i$, was calculated from the returned light intensity.

2.4 *Determination of Extinction-to-Backscatter Ratio from Lidar Measurements*

For each laser shot an average column attenuated backscatter coefficient, $\overline{\beta'_i}$, and an average column extinction coefficient, $\overline{\sigma}_{ext_i}$, can be defined by

$$\overline{\beta'}_i = \frac{\int_{aircraft(r=0)}^{surface} \beta'(r)_i dr}{\int_0^{surface} dr} \tag{6}$$

$$\overline{\sigma}_{ext_i} = \frac{\delta_i}{\int_{aircraft(r=0)}^{surface} dr} \tag{7}$$

These two quantities are average values for the entire column of air and smoke between the aircraft and the ocean. The individual magnitudes of these two quantities are not average

values in the smoke because the column includes smoke-free air above and below the smoke plume. It is the ratio of these two parameters that is of significance.

Figure 2 shows a sample scatter plot of $\overline{\sigma}_{ext_i}$ versus $\overline{\beta_i'}$ Each point in this plot is a 1 s (10 shot) average. If we assume that the extinction and (unattenuated) backscatter are related by an expression of the form

$$\sigma_{ext} = C\beta \tag{8}$$

Then the attenuated backscatter coefficient would also obey this relationship at low values of beam attenuation. Figure 2 suggests that provided $\overline{\sigma}_{ext_i}$ and $\overline{\beta_i'}$ are not too large, they are related linearly; for the straight line shown in Figure 2 the slope (C) is equal to 38 str.

As explained above, the attenuated backscatter coefficient, $\beta'(r)$, is determined by comparing the returned light intensity from the smoke to the returned light intensity from clear air at the same range. Once $\beta'(r)$ and C are known, the range-dependent extinction coefficient $\sigma_{ext_i}(r)$ can be calculated from[22]:

$$\sigma_{ext_i}(r) = \beta_i'(r)\left[\frac{1}{C} - 2\int_{\substack{aircraft \\ (r=0)}}^{r}\beta_i'(r)dr\right]^{-1} \tag{9}$$

2.5 *Determination of Specific Extinction of Smoke*

The specific extinction, A_e (units: $m^2\ g^{-1}$), of the smoke is defined as the ratio of the extinction coefficient (units: m^{-1}) to the particulate mass concentration, ρ_a (units: $g\ m^{-3}$). Teflon filters were used to determine the mass concentrations. Measurements from the optical extinction cell were averaged over the times that the filters were exposed to the smoke, to determine the extinction coefficient.

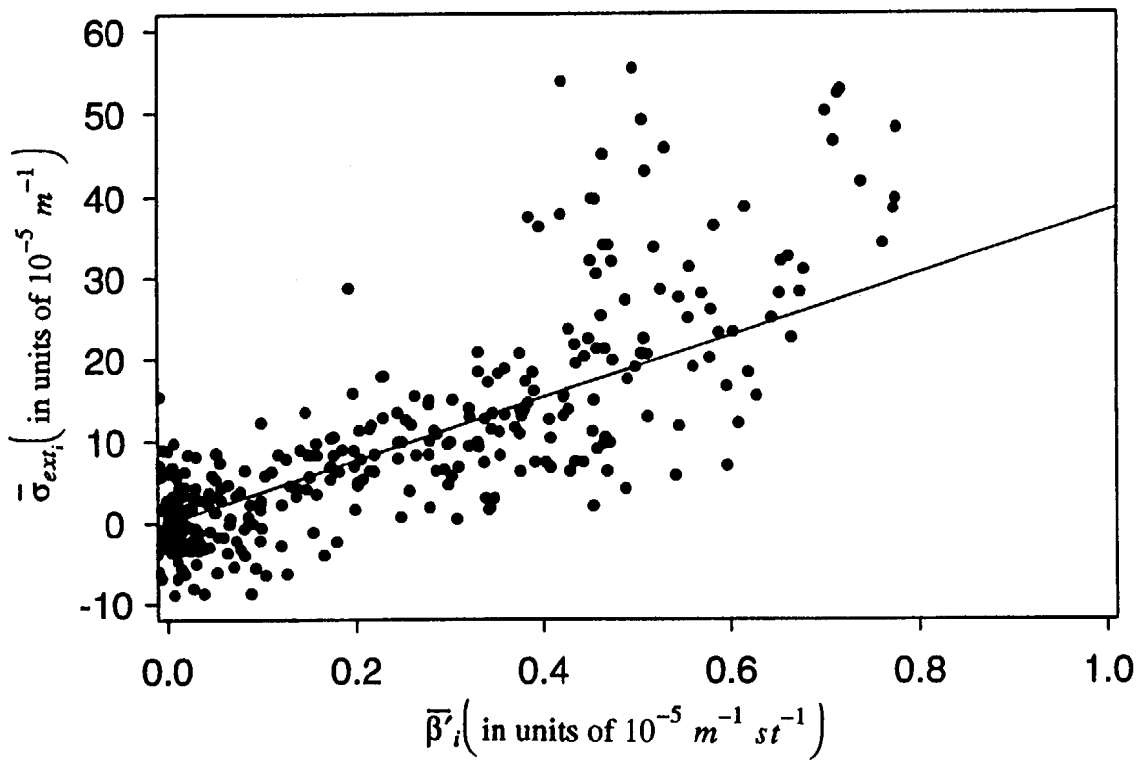

Figure 2. Scatterplot of average column extinction coefficient ($\bar{\sigma}_{ext_i}$) versus the average column attenuated backscatter coefficient ($\bar{\beta}_i$). The line shown is the best fit of points with extinction coefficient <35 x 10^{-5} m^{-1}.

2.6 *Determination of Particulate Mass Distributions and Fluxes of Smoke*

Once the above quantities have been calculated they can be combined to derive the mass concentrations of particles in the smoke, $\rho_i(r)$, as a function of range r for each laser shot

$$\rho_i(r) = \frac{\sigma_{ext_i}(r)}{A_e} \tag{10}$$

A lidar cross section through the smoke plume can be integrated to obtain the total mass of particles in the smoke and, using the wind speed perpendicular to the cross section, V (which is measured aboard the aircraft), the instantaneous mass flux of smoke particles through the cross section can be calculated from

$$\dot{m} = V \iint \rho_i(r) r dr d\theta \tag{11}$$

where $rdrd\theta$ is an elemental area normal to the wind vector at range r.

3. RESULTS

3.1 *Summary of Flight Operations on 7 August 1993*

We received notice that the first NOBE burn was to begin in about 1 hour and took off from St. John's at 1107 hours local time. We arrived at the burn site at about the time a fog was forming and spent about 1 hour orbiting the area downwind of the ships. During this time background measurements were made with one PUF sample, one SUMMA canister, one quartz filter, and a pair of Teflon filters. The flight was then aborted due to persistent fog and several hours later the burn was canceled for that day.

3.2 *Summary of Flight Operations on 12 August 1993*

(a) **Overview of First NOBE Burn (UW Flight 1617).** After receiving the "1 hour till burn" notice we departed St. John's at 0800 hours local time. Visibility at the burn site was good with a broken stratus cloud deck between 120 and 250 m above mean sea level

(MSL). Two background samples (1 PUF, 2 quartz, and 2 pairs of Teflon filters) were collected about 1.5 km downwind of the backup boom between 0821 and 1006 hours. Numerous passes were made at several levels about 1.5 km downwind in order to get background data on the plumes of the various ships in the area. Ship plumes were observed visually and measured at 120 m MSL (just below cloud base). However, ship plumes were neither seen nor detected above the clouds.

When the first NOBE burn began (at about 1030 hours), the smoke plume was observed to rise quickly above the cloud deck; it is therefore believed to have been relatively free of contamination from the surrounding ship plumes. Our initial sampling of the smoke concentrated on the region of plume about 1.5 km downwind of the fire. To obtain a concentrated smoke sample for a PUF (to get a good measure of the PAH content of the smoke) three successive bag samples were collected (between 1056 and 1108 hours) using the aircraft's 2.5 m^3 grab-bag sampling system. An additional bag sample was collected 1.5 km downwind (at 1039 hours) for determination of emission factors (EF) at that location. We then climbed to 1,200 m MSL and made a pass over the plume to get a lidar cross-section at 1.5 km downwind. Passes through the plume were then made at about 5, 8, 14, 18, 24 and 32 km downwind to measure the dilution of the smoke with distance from the fire. During these passes bag samples were collected (for quartz and Teflon filters and SUMMA canisters) at 5 and 32 km downwind. After taking the 32 km downwind sample, we climbed to 1,200 m and made a pass along the plume centerline to obtain a lidar profile of the plume. At the end of this pass (1157 hours) the burn was nearly complete so we returned to St. John's to refuel and prepare for the second burn of the day.

The plume from the first burn exhibited an interesting dispersion pattern. Most of the smoke rose to between 250 and 600 m MSL and was transported northward by the low-level southerly winds. However, six large puffs of smoke rose above the main body of the plume, reaching a height of about 1,200 m. At this level the winds were westerly and the

six puffs sheared off and moved to the east while the main plume continued northward. When we arrived on site for the second burn the plume from the first burn could still be seen in the distance (out to the NE horizon).

(b) **Overview of Second NOBE Burn (UW Flight 1618).** We arrived at the burn site at about 1350 hours. Since ignition was imminent, we collected only one background bag sample for a SUMMA canister (more background samples were collected after the burn). After ignition we collected the first smoke sample at a point 3 km downwind, concentrating on collecting three bags for a good PUF sample and an additional single bag for emission factor measurements. We then climbed to 1,500 m for several lidar cross section measurements of the plume at 5, 7 and 10 km downwind, and a lidar run along the length of the plume centerline. At 1458 and 1518 hours, single bag samples were collected (for quartz and Teflon filters and SUMMA canisters) at 14 and 24 km downwind, respectively. We then sampled at three levels in the smoke at 10 km downwind for cross-sectional measurements of fluxes in the plume. Another lidar run along the plume centerline was then made at an altitude of 1,800 m, followed by a return pass in the smoke down the center of the plume for continuous *in situ* measurements. Finally, a smoke sample was collected at 450 m and 19 km downwind, and several bags were collected for background concentrations out of the smoke.

A chronology of the flights listing the times of significant events and the air volumes of the grab samples is given in Tables 1 and 2. Figures 3 and 4 show the flight tracks for the two flights.

The smoke plumes from both test burns rose quickly to ~200–400 m above mean sea level and then rose more slowly. During the first burn a low, patchy cloud layer located at the top of the marine boundary layer (~200–250 m MSL) covered the area. The smoke plume rose through this cloud layer and was then carried to the northeast by the wind. Later in the day, when the second burn started (at 1408 hours local time), the marine

TABLE 1. Summary of Significant Events for the First NOBE Burn on 12 August 1993 (UW Flight 1617)

LOCAL TIME	EVENT	PUF's		QUARTZ FILTERS		PM 3.5 FILTERS		PM 10 FILTERS		SUMMA SAMPLES	
		Sample Number	Cumulative Volume (liters)	Sample Number	Cumulative Volume (liters)	Sample Number	Cumulative Volume (liters)	Sample Number	Cumulative Volume (liters)	Can Number	Final Pressure
0530	Ground power on to aircraft to warm up gas instruments										
0746	Aircraft engine start										
0759	Takeoff										
0812–0819	Descent from 1400 m to 15 m for temperature sounding; cloud tops at 250 m, bases approx 140 m										
0821–0845	1st Background samples (ship plumes detected)										
0821	1st BAG, 1.6 km downwind, 120 m	NFP3	1207	NFQ2	114	NF3	108	NF4	116	---	
0827	2nd BAG, 1.6 km downwind, 120 m	"	2250	"	180	"	200	"	220	EPS-53	30 PSI
0833	3rd BAG, 1.6 km downwind, 120 m	"	3128	"	248	'	328	"	343	---	
0840	4th BAG, 1.6 km downwind, 120 m	"	3998	"	304	"	428	"	445	EPS-132	
0840–0845	Sounding from 30 to 600 m										
0845	5th BAG	"	4973	"	361	"	540	"	561	---	
0914–0922	Sounding from 30 to 600 m										
0935	Crosswind pass 1.6 km downwind of ships at 250 m; no ship plumes at this level										
0954–1006	2nd Background samples (at 120 m altitude and 3 km downwind of burn)										

TABLE 1 (CONTINUED)

LOCAL TIME	EVENT	PUF's		QUARTZ FILTERS		PM 3.5 FILTERS		PM 10 FILTERS		SUMMA SAMPLES	
		Sample Number	Cumulative Volume (liters)	Sample Number	Cumulative Volume (liters)	Sample Number	Cumulative Volume (liters)	Sample Number	Cumulative Volume (liters)	Can Number	Final Pressure
0954	1st BAG	---		NFQ3	158	NF5	330	NF6	349	---	
1006	2nd BAG	---		"	366	"	558	"	586	---	
1030–1033	Sounding from 60 to 450 m										
Approx 1030	Fire ignited, plume rose immediately above cloud tops										
1039	(Smoke sample collected 1.6 km downwind, 230 m altitude. BAG sample for emission factor measurement)	---		NFQ4	325	NF7	300	NF8	315	EPS-27	30 PSI
1046	2nd plume pass										
1053	3rd plume pass, bag filled but missed plume, aborted bag										
1056–1108	Smoke samples collected (1.6 km downwind, 120 m for PUF sample)										
1056	1st BAG	NFP4	870	NFQ5	109	NF9	100	NF10	111	EPS-151	30 PSI
1102	2nd BAG	"	1718	"	228	"	207	"	232	---	
1108	3rd BAG	"	2655	"	360	"	326	"	366	EPS-6	
1116–1121	Sounding from 60 to 1220 m. Burn about half over										
1122–1123	Lidar cross section of plume from 1220 m										

TABLE 1 (CONTINUED)

LOCAL TIME	EVENT	PUF's		QUARTZ FILTERS		PM 3.5 FILTERS		PM 10 FILTERS		SUMMA SAMPLES	
		Sample Number	Cumulative Volume (liters)	Sample Number	Cumulative Volume (liters)	Sample Number	Cumulative Volume (liters)	Sample Number	Cumulative Volume (liters)	Can Number	Final Pressure
1127	Smoke sample collected, (5 km downwind, 1 BAG)	---		NFQ6	281	NF11	255	NF12	264	EPS-22	30 PSI
1129	Plume pass ~8 km downwind										
1132	Plume pass ~ 14 km downwind										
1134	Plume pass ~ 18 km downwind										
1139	Plume pass ~ 24 km downwind										
1143	Smoke sample (~ 32 km downwind, 1 BAG)	---		NFQ7	339	NF15	341	NF16	331	GVRD430	30 PSI
1147–1157	Lidar pass along plume centerline at 1220 km										
1158	Return to St. John's										
1216	Engines off										

TABLE 2. Summary of Significant Events for the second NOBE Burn on 12 August 1993 (UW Flight 1618)

LOCAL TIME	EVENT	PUF's		QUARTZ FILTERS		PM 3.5 FILTERS		PM 10 FILTERS		SUMMA SAMPLES	
		Sample Number	Cumulative Volume (liters)	Sample Number	Cumulative Volume (liters)	Sample Number	Cumulative Volume (liters)	Sample Number	Cumulative Volume (liters)	Can Number	Final Pressure
1327	Engines on										
1336	Take off										
1400	Background sample (SUMMA only)	---		---		---		---		EPS 223	30 PSI
1408	Fire ignited										
1413–1424	First smoke sample (3 km downwind)										
1413	1st BAG	NFP5	840	NFQ10	107	NF17	104	NF18	136	EPS 226	30 PSI
1419	2nd BAG	"	1748	"	223	"	215	"	294	---	
1424	3rd BAG	"	2580	"	330	"	316	"	438	EPS 220	30 PSI
1432	2nd smoke sample (3 km downwind for emission factors, 1 BAG			NFQ11	300	NF19	292	NF20	412	AB02	30 PSI
1438–1439	Lidar cross section of plume ~ 3 km downwind										
1441–1442	Lidar cross section of plume ~ 8 km downwind										
1444–1445	Lidar cross section of plume ~ 5 km downwind										
1446–1451	Lidar run along plume centerline										
1458	Smoke sample (14 km downwind, 1 BAG)	---		NFQ12	323	NF21	315	NF22	457	EPS 100	30 PSI
1506–1512	Continuous in plume sampling along centerline										

TABLE 2 (CONTINUED)

LOCAL TIME	EVENT	PUF's		QUARTZ FILTERS		PM 3.5 FILTERS		PM 10 FILTERS		SUMMA SAMPLES	
		Sample Number	Cumulative Volume (liters)	Sample Number	Cumulative Volume (liters)	Sample Number	Cumulative Volume (liters)	Sample Number	Cumulative Volume (liters)	Can Number	Final Pressure
1518	Smoke sample (1 BAG, 24 km downwind at altitude of 60 m (below smoke). Nothing detectable above background)	---		NFQ13	268	NF23	259	NF24	382	EPS 24	30 PSI
1528–1538	Cross section sample for fluxes at 10 km downwind:										
1528	1st BAG at 335 m	NFP6	683	NFQ14	109	NF25	106	NF26	157	GVRD433	20 PSI
1532	2nd BAG at 443 m	"	1402	"	213	"	206	"	305	EPS 163	30 PSI
1538	3rd BAG at 535 m	"	2220	"	332	"	320	"	472	#11568	30 PSI
1539–1547	Sounding up to 1830 m										
1550–1558	Lidar run along plume centerline										
1602–1610	Continuous sampling in smoke along plume centerline										
1610	Smoke sample (at 450 m, 19 km downwind)	---		NFQ15	291	NF27	277	NF28	411	#13592	30 PSI
1623–1638	Background sample (out of smoke)										
1623	1st BAG	NFP7	~ 1000	NFQ16	~ 120	NF29	~ 115	NF30	~ 170	EPS 164	30 PSI
1627	2nd BAG	"	~ 1300	"	~ 240	"	~ 230	"	~ 360	---	
1634	3rd BAG	"	2040	"	368	"	354	"	525	#13600	
1638	4th BAG	"	2933	"	481	"	462	"	684	___	
1640	Head back to St. John's										

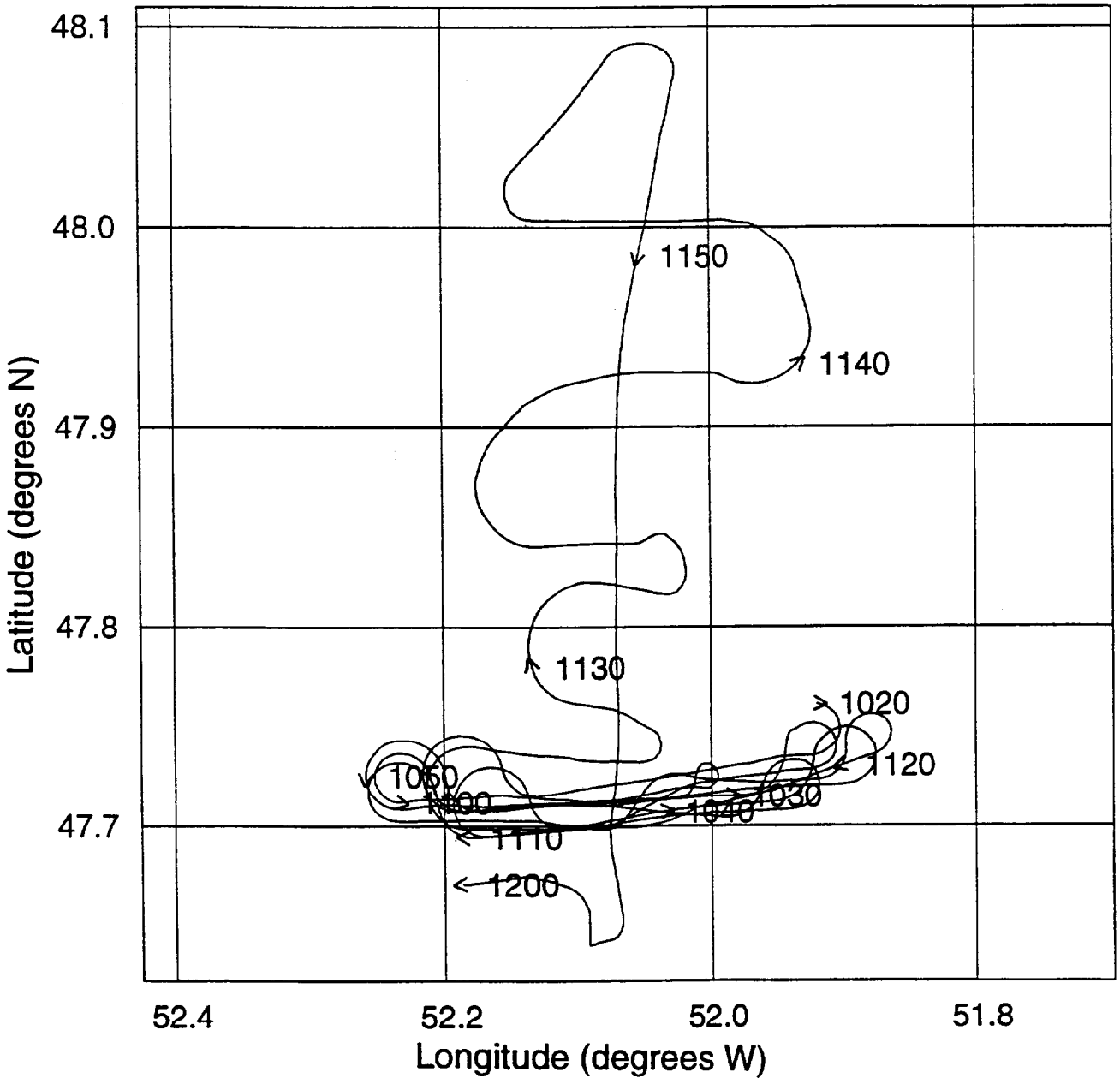

Figure 3. Flight track of University of Washington research aircraft during the first NOBE burn (numbers along track indicate local time).

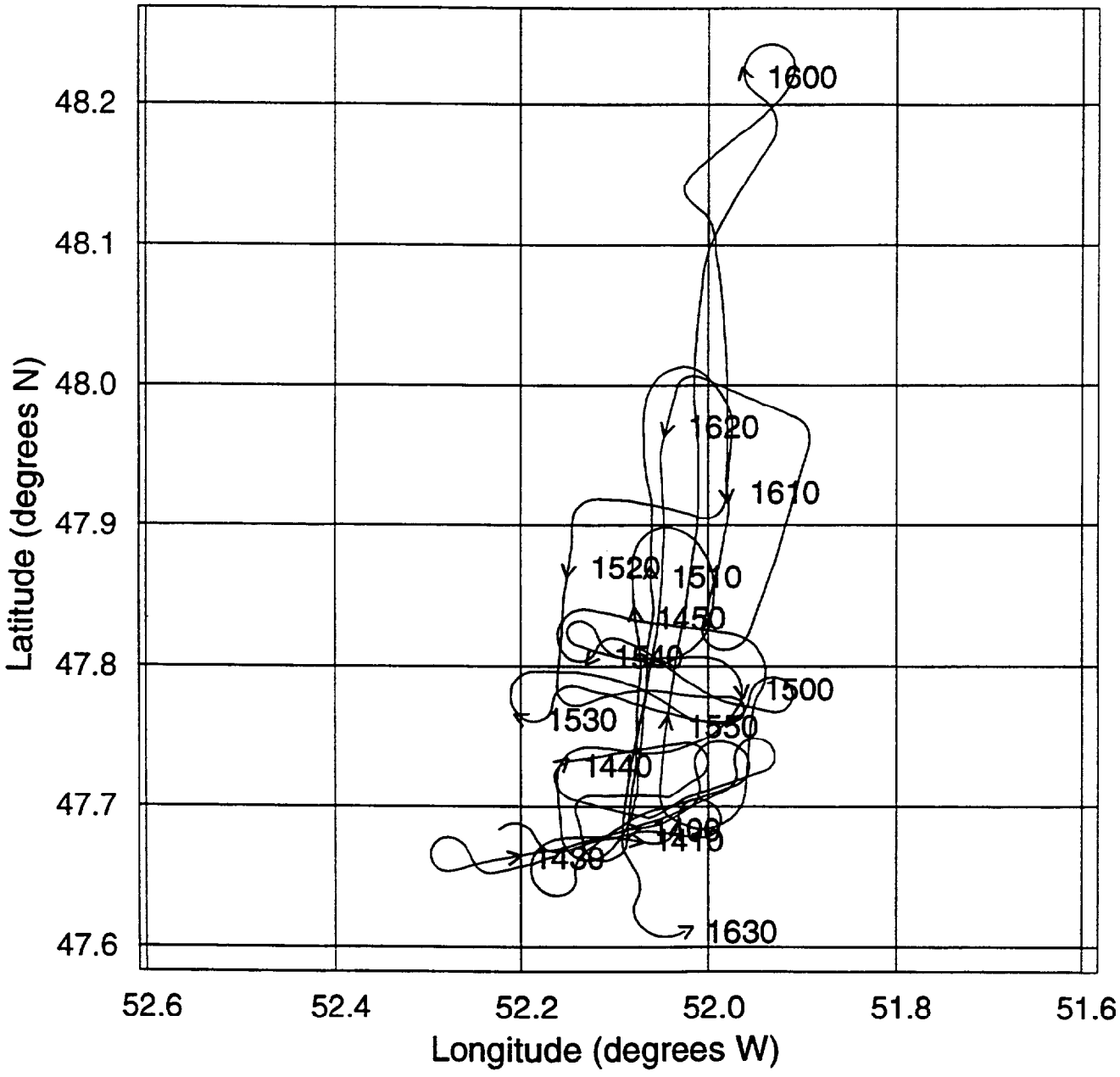

Figure 4. Flight track of University of Washington research aircraft during the second NOBE burn (numbers along track indicate local time).

boundary layer had risen to a height of ~450–500 m MSL and the clouds had disappeared. The plume from the second burn rose well above the top of this boundary layer.

The winds were southerly at the surface, but veered to west-southwesterly with height. Therefore, as the smoke rose it gradually curved towards the northeast, and slanted upwards to the east. At ~30 km downwind some portions of the plume rose to over 800 m, possibly due to solar heating of the smoke[16].

3.3 *Particle Mass Concentrations and Chemical Composition of the Smoke*

For both of the NOBE burns particle mass concentrations of ~800–1000 $\mu g\ m^{-3}$ were common near (~1.5 km) the fires (Figure 5). However, after 1–1.5 hours of travel time downwind, the particle mass concentrations approached the EPA standard (24 h average) of 150 $\mu g\ m^{-3}$. Mass concentrations were measured using filters with 3.5 μm aerodynamic diameter cut points, but these filters may have collected some particles larger than 3.5 μm geometric diameter. Measurements in the smoke of the Kuwait oil fires showed that particles in this size range had geometric diameters 6 to 31 times larger than their aerodynamic diameters[23]. Figure 5 shows particle mass concentrations derived from the PCASP measurements. The volume distributions from the PCASP were integrated and an 'effective density' for each of the eight samples was calculated. This is the particle density required to match the mass from the filters. The mean value of the effective density for the eight samples was $1.47 \pm 0.34\ g\ cm^{-3}$. The volume concentrations from the PCASP were then multiplied by the average effective density to give the mass concentrations shown in Figure 5.

Our analysis shows that the PCASP can be used to estimate aerosol mass concentrations provided it is 'calibrated' to the aerosol sampled. This is promising, because a continuously operating PCASP can provide considerably more information than a few discrete bag samples. It also provides improved spatial resolution of mass concentration gradients.

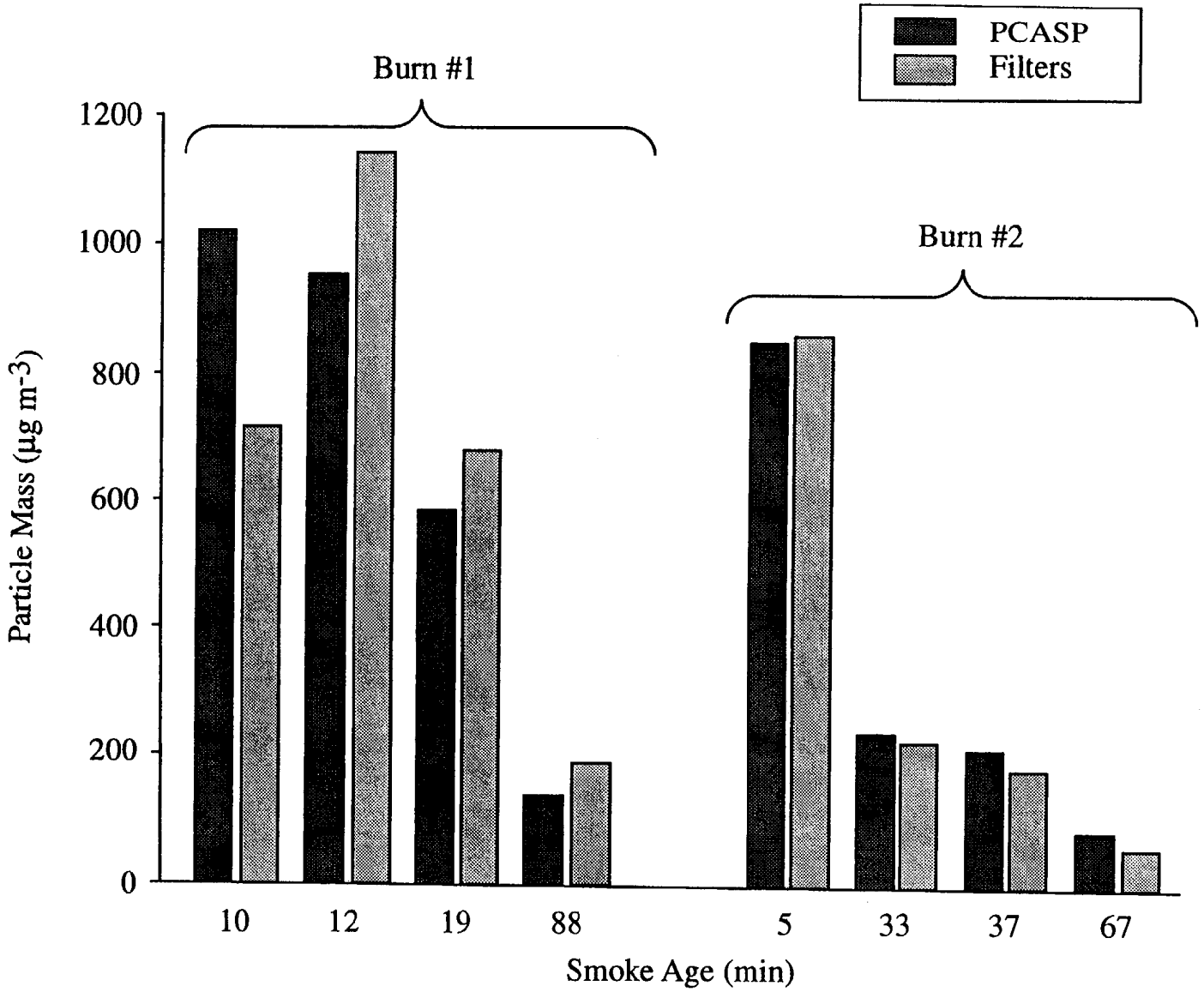

Figure 5. Particle mass concentrations produced by the first and second NOBE burns.

Samples of the smoke collected on quartz filters were analyzed for their elemental and organic carbon contents (Figure 6). With the exception of the measurement at 88 minutes smoke travel time downwind, ~76% of the mass of the smoke particles was elemental carbon, ~8% was organic carbon, and 16% was unidentified. The measurement made at 88 minutes shows considerably more organic and unidentified fractions. It is uncertain whether there was enough organic carbon present in the vapor phase to begin with to account for the additional condensed organics indicated by that sample or whether the sample was contaminated.

3.4 *Emission Factors for Particles*

Emission factors quantify the relative amounts of various species emitted by a fire. Emission factors for a variety of chemical species can be derived from airborne measurements using the carbon balance method[17,24], which requires instantaneous measurements of the concentrations of all the major carbon-containing species at a point in the smoke plume and knowledge of the carbon fraction of the fuel (0.858 in this case).

Table 3 shows the concentrations and calculated emission factors for CO_2, elemental carbon, organic carbon, VOCs, and particulate mass for the two NOBE burns. The emission factor for sub-3.5 μm particulate mass (87 ± 15 g kg^{-1}) suggests a lower combustion efficiency (i.e., more particulate emissions) for the NOBE burns than for the Kuwait oil pool fires (~50 g kg^{-1})[24]. In pan fire tests Benner et al.[6] reported total (all sizes) particulate emission factors that increased from 35 to 80 g kg^{-1}, as the fuel layer thickness increased. Koseki and Mulholland[25] found in pan fire tests a three-fold increase in the emissions factor of particles of all sizes from ~60 to ~180 g kg^{-1} as the diameter of the fire increased from 0.6 m to 3 m. Clearly, there are many factors that could affect the combustion efficiency of oil burning on water.

The measured emission factor for elemental carbon for the NOBE burns was 66 ± 18 g(C) kg^{-1} and for organic carbon in condensed form it was 7 ± 3 g(C) kg^{-1}. The emission

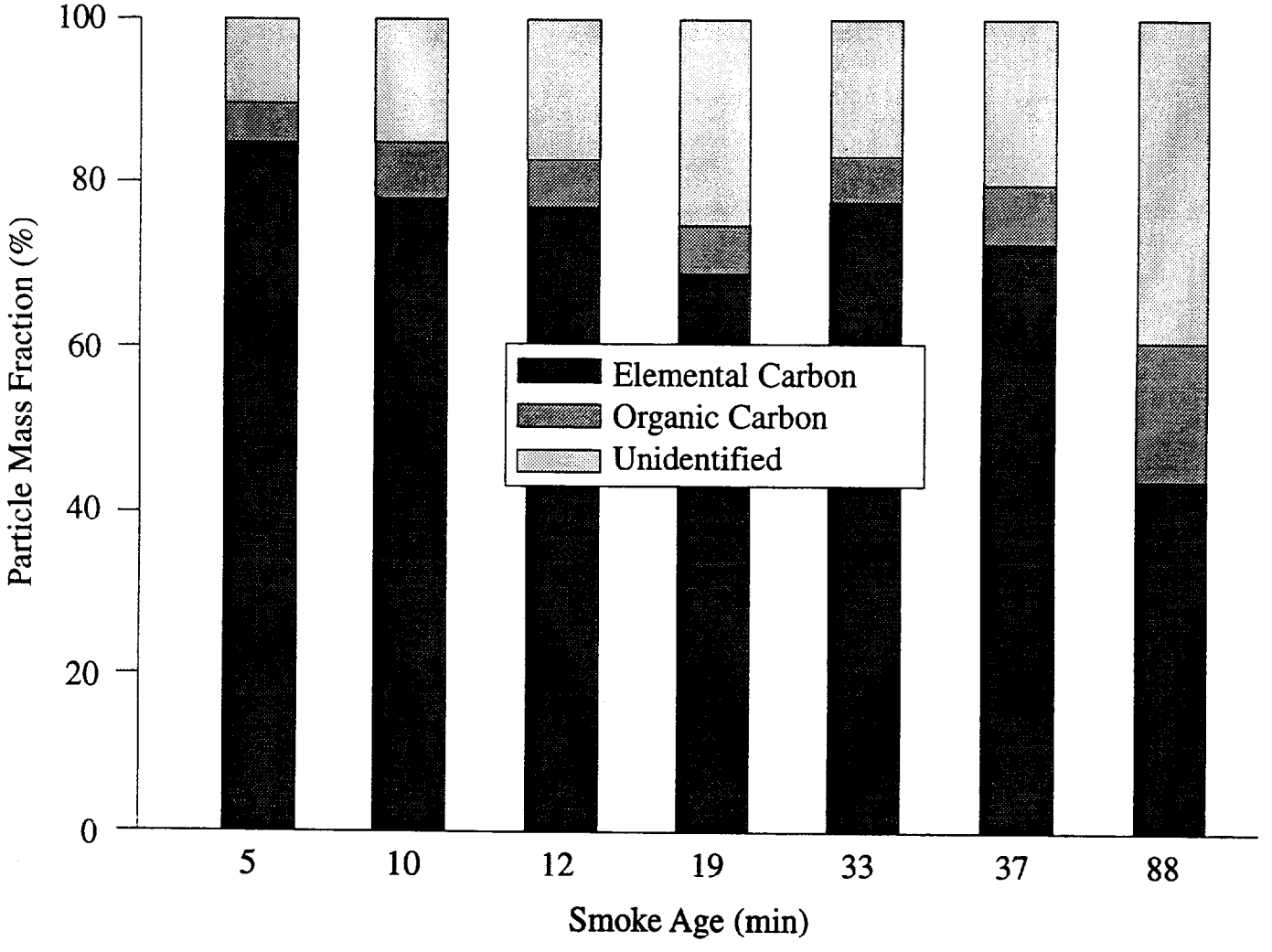

Figure 6. Mass fractions of elemental carbon, organic carbon and other (unidentified) materials in the smoke particles from the NOBE burns.

TABLE 3. Concentrations and emission factors (EF) (in grams of carbon per kilogram of fuel) for excess carbon dioxide (CO_2), elemental carbon in particles (EC_a), organic carbon in particles (OC_a), Volatile Organic Compounds (VOCs), and for particles <3.5 μm diameter (EF is in grams of particulate mass per kilogram fuel). Results were derived from seven filter exposed to smoke at various distances downwind in the NOBE burns.

		CO_2		EC_a		OC_a		VOC		Particulate Mass	
NOBE Burn	Smoke Age (min)	Concentration (ppm)	EF ($g(C)kg^{-1}$)	Concentration ($\mu g\ m^{-3}$)	EF ($g(C)kg^{-1}$)	Concentration ($\mu g\ m^{-3}$)	EF ($g(C)kg^{-1}$)	Concentration ($\mu g\ m^{-3}$)	EF ($g(C)kg^{-1}$)	Concentration ($\mu g\ m^{-3}$)	EF ($g(C)kg^{-1}$)
1st	10	17.2	774	555	49	53	4.7	185	16.4	710	63
1st	12	17.9	763	878	74	70	5.9	28	5.7	1139	96
1st	19	9.8	752	510	77	46	6.9	60	9.1	735	111
1st	88	3.8	794	88	36	34	14.1	0	0	199	82
2nd	5	13.2	758	721	82	43	4.9	6	0.7	850	96
2nd	33	3.6	750	209	86	16	6.6	6	1.2	195	80
2nd	37	3.7	779	142	59	13	5.5	2	0.8	195	81
Mean			767		66		7		5		87
Standard Deviation			16		18		3		6		15

factors measured in Kuwait for two pool fires were significantly lower[24]; for elemental carbon they were 16 and 28 g(C) kg^{-1} and for organic carbon in condensed form they were 1.6 and 2.8 g(C) kg^{-1}.

3.5 *Specific Extinction of Smoke*

The mean value of the specific extinction (A_e) derived from all of the filter samples was 8.7 m^2 g^{-1} (at λ = 0.538 μm). Similar results were obtained by Bruce et al.[26], who determined a specific extinction coefficient of 6.97±0.31 m^2 g^{-1} for diesel soot at λ = 0.488 μm. Roessler and Faxvog[27] measured a specific extinction coefficient of 9.8±0.8 m^2 g^{-1} for acetylene smoke at λ = 0.515 μm.

3.6 *Spatial Distribution and Concentrations of Gases in the Smoke Plume*

Measurements from several fast-response instruments aboard the aircraft were examined for each cross-section of the smoke plumes. Figure 7 shows an example. To detect gases from the plume, the Li-Cor CO_2 analyzer was used, and for smoke particles the cumulative total from the PCASP-100X was used. As the aircraft entered the plume both the CO_2 and particle concentrations increased sharply. No evidence was found for the preferential diffusion of gases (compared to particles) from the smoke plumes.

The air within the smoke plume was characteristic of the air near the surface around the fire itself, rather than the air surrounding the smoke plume at any distance downwind. Evidence for lofting of surface air is provided by the difference in the value of the water mixing ratio between air in and out of the smoke for plume penetrations above and below the boundary layer top. The water mixing ratio in the boundary layer was ~7 g kg^{-1}, but dropped sharply to ~3-4 g kg^{-1} above the boundary layer (Figure 8a). When the aircraft made a low-level pass through the smoke plume (e.g., at 200 m) (Figure 8c) the mixing ratio in the smoke was unchanged from the value outside of the plume (~7 g kg^{-1}). However, when a pass was made above the boundary layer (e.g., at 700 m) (Figure 8b)

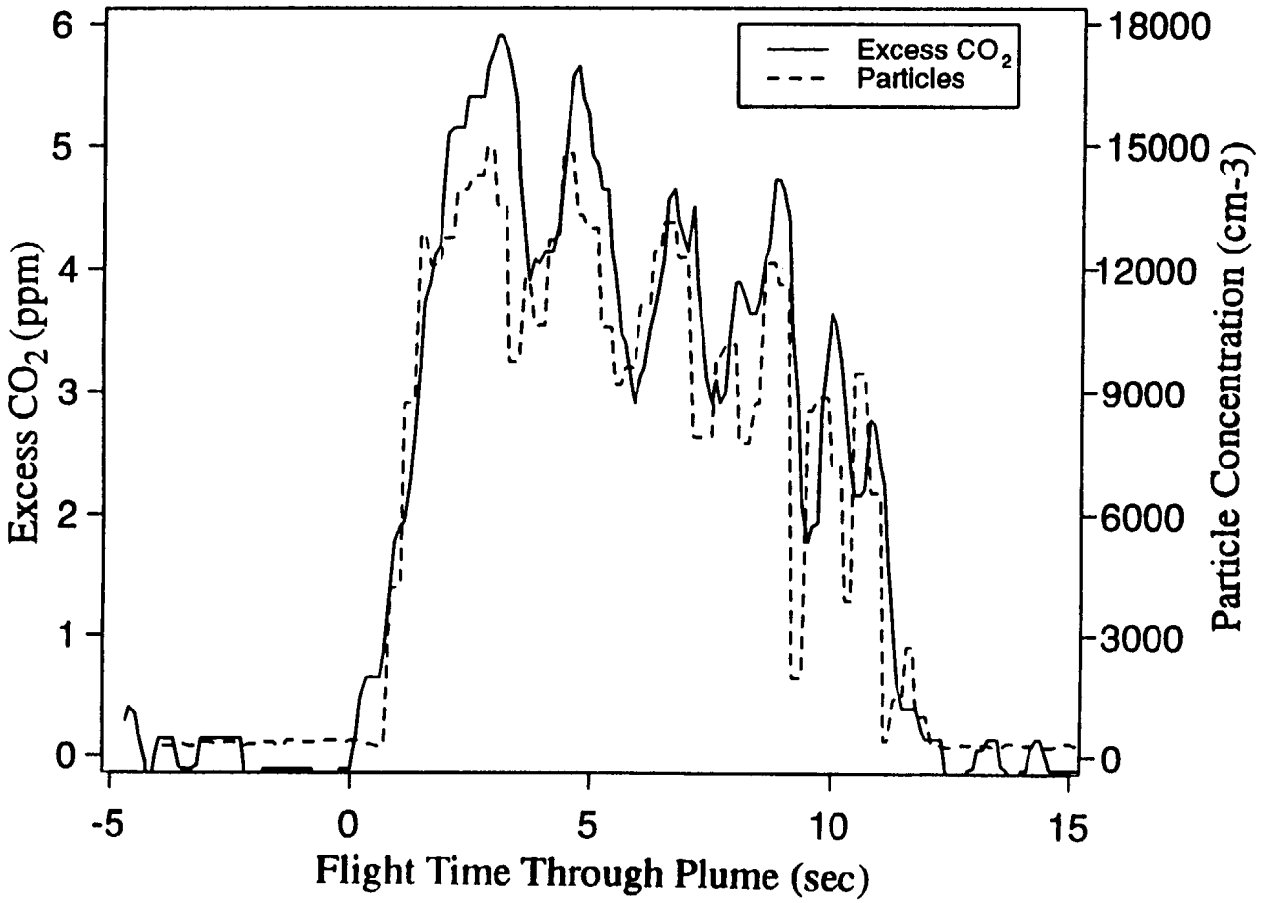

Figure 7. Comparison of gaseous and particulate concentrations for a typical plume penetration. CO_2 data was shifted 1 sec. to account for a time measurement lag.

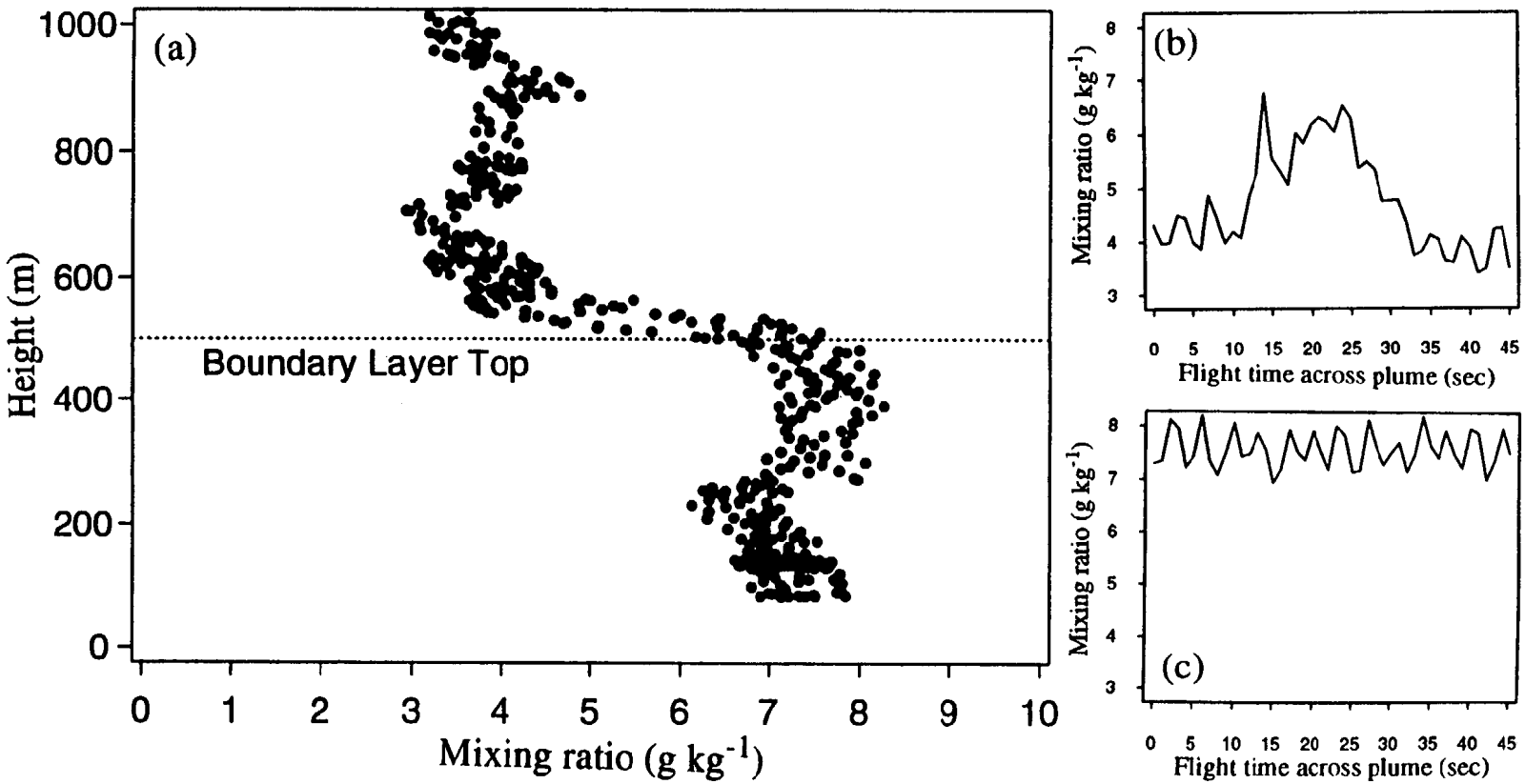

Figure 8. Vertical profile of water mixing ratio. Points are 1 sec. averages. Height is above sea surface. Boundary layer top is indicated.

the mixing ratio inside the smoke plume jumped sharply from lower values outside the smoke (~4 g kg^{-1}) to values more characteristic of the boundary layer air below (~6–7 g kg^{-1}). Since water production from combustion is far too small to account for the elevated concentrations in the smoke, the air in the smoke downwind must have originated from near the source of the fire.

This aspect of the plume is relevant to the calculation of emission factors, since the background concentrations of CO_2 were not constant with height. In the air above the boundary layer the CO_2 concentration were ~3–4 ppm lower than in the boundary layer. Our emission factor calculations are based on measurements of the excess (i.e., above ambient) concentrations of CO_2 in the plume. Hence, for portions of the plume that extended above the boundary layer, the ambient CO_2 concentrations used in the calculation of emission factors was that in the boundary layer.

The lofting of surface air with high humidity into the smoke plume also has implications for the potential lifetime of the smoke. If the convective column produced by the burning of crude oil lofts water vapor from the surface, this will increase the chance that the plume will become supersaturated with water, form a cloud, precipitate, and remove particles in the plume to the surface through precipitation scavenging.

The highest concentration of excess CO_2 measured in the smoke plumes was ~40 ppm, which was located nearest to the fire; the concentration fell off gradually as the plumes dispersed. Excess CO_2 typically fell below the discrimination limit (~1 ppm) about ~25–30 km downwind.

A gaseous pollutant of potential concern is NO_x. Photolysis of NO_2 is the chain initiation step in the photochemical production of O_3, peroxyacetyl nitrate, and other secondary pollutants. NO_x concentrations produced by the NOBE burns were fairly low. The ratio of NO_x (ppb) to excess CO_2 (ppm) was typically 0.3–0.4. This means that the peak NO_x concentration was ~15 ppb and through most of the plume the NO_x concentrations were only a few parts per billion. *In situ* burning of crude oil should not

result in significant production of secondary pollutants through photochemical reactions with NO_x. The low concentrations are probably due to a relatively low flame temperature and the low nitrogen content of the fuel. Little to no atmospheric nitrogen would be fixed.

The measured emission factor for organic carbon in the vapor phase was highly variable. Some of the canister samples used to calculate this quantity could have been contaminated with ship exhaust, including some samples taken as background measurements. However, it is not likely that much unburned hydrocarbon vapor escaped the flame zone.

3.7 *CO_2 Flux Determined from in situ Measurements*

A crude estimate of the total flux of CO_2 was made using *in situ* data from a multiple pass cross section. During the second NOBE burn, starting at 15:28 hours local time, the UW aircraft made three passes through the plume at 10 km downwind at altitudes of 385, 443, and 535 m. The bottom and top of the plume was estimated from lidar data to be at 300 and 650 m. By examining data from fast response instruments and the airspeed of the plane, the width of each pass and the area of the plume cross section were estimated. The excess CO_2 was approximated for the cross section by averaging the data from the Li-Cor 6262 CO_2 analyzer measured during each pass. The wind perpendicular to the flight track was 8 m s^{-1}. This allows calculation of the mass flux of CO_2. Next, the flux of carbon was estimated by assuming that 89% of carbon emitted was in the form of CO_2. This value was determined by an overall carbon budget analysis for both NOBE burns. To convert from carbon mass flux to total fuel consumption rate the carbon fraction of the fuel was assumed to be 0.858 kg (C) per kilogram of oil. The density of the oil was 0.84 g cm^{-3}. A combination of these quantities yields a fuel consumption rate of 720 liters min^{-1}. This compares reasonably well with the reported pump rate of 560 liters min^{-1}, and supports our assertion that large amounts of CO_2 did not "escape" from the plume.

3.8 *Polycyclic Aromatic Hydrocarbons*

Smoke samples collected on the PUFs were analyzed for PAHs. Details of the analysis procedure are given by Fingas et al[28]. The results are shown in Table 4.

The heaviest measured total concentration of PAHs was for a background sample taken downwind of the ship exhausts (NFP1). The final line in Table 4 shows the amount of the smoke mass that was composed of PAH (in micrograms of PAH per gram smoke). When correcting for background concentrations the heavy sample (NFP1) was not used, thus the indicated amounts of PAHs in the smoke should be upper limits. The first two values (650 and 770 $\mu g\ g^{-1}$) are quite low. The third is much higher (6400 $\mu g\ g^{-1}$), and is comparable to the values reported by Benner et al[6]. The most prevalent compound was napthalene. Benner et al[6], who used the same type of crude oil (Alberta Sweet) burned in NOBE, did not measure any napthalene from their pan fire tests. A species not present above the detection limit in the NOBE smoke was benzo(a)pyrene, which is often used as a surrogate indicator compound to characterize gross PAH levels[29]. Clearly this would not be an appropriate choice for the smoke from the NOBE fires.

3.9 *Emission Factors for Gases*

The derived emission factors (in grams of carbon per kilogram of fuel) for CO_2 and VOCs for the NOBE burns are listed in Table 3. The emission factor for CO_2 for the NOBE burns (767 g (C) kg^{-1}) is only slightly less than those reported by Laursen et al[24] for two pool fires in Kuwait (824 and 805 g (C) kg^{-1}). The lower value for the NOBE burns indicates lower combustion efficiency, since the carbon fractions of the two crudes were not significantly different.

The average value of the ratio of concentration of CO to CO_2 in the smoke from the NOBE burns was 0.017. This is similar to the values measured by Koseki and Mulholland[25] in pan experiments with oil floating on water. During one of their test burns the CO/CO_2 ratio varied almost linearly in time from ~0.012 to ~0.024, with a higher value

TABLE 4. Concentrations of Polycyclic Aromatic Hydrocarbons (PAHs), in μg m^{-3}. Measured on August 7 and on August 12 in the two NOBI Burns. Sample Types are: Background (Bkgd), Smoke (Smk), and Blank (Blank). NA and ND Stand for "Not Applicable" and Not Detected"

	AUGUST 7	NOBE Burn 1 (AUGUST 12)			NOBE Burn 2 (AUGUST 12)			Controls			
Sample Type	Bkgd	Bkgd	Smk	Bkgd	Smk	Smk	Blank	Blank	Blank	Blank	Blank
Sample ID	NFP1	NFP3	NFP4	NFP7	NFP5	NFP6					
Sample Size (m^3)	1.522	4.972	2.655	2.932	2.580	2.200	NA	NA	NA	NA	NA
Comments	Some ship exhaust	Some ship exhaust	1.6 km downind	No ship exhaust	3 km downwind	10 km downwind	Loaded, no air sampled		Not loaded, no air sampled	Control for trip blank	Control for NPF6, 7
Compound	**Concentrations (μg m^{-3})**										
Naphthalene	0.46	0.14	0.41	0.11	0.22	0.34	0.43	ND	0.79	ND	ND
1-Methylnapthalene	0.66	0.16	0.36	0.19	0.27	0.49	0.40	ND	0.75	ND	ND
2-Methylnapthalene	0.34	0.08	0.18	0.10	0.15	0.24	0.17	ND	0.37	ND	ND
Biphenyl	0.22	<0.05	0.06	0.05	0.08	0.15	0.06	ND	<0.1	ND	ND
2.6-Dimethylnaphthalene	0.25	0.05	0.12	0.09	0.13	0.19	0.10	ND	0.17	ND	ND
Acenaphthalene	<0.05	<0.05	<0.05	<0.05	<0.05	<0.05	<0.05	ND	<0.1	ND	ND
Acenaphthene	0.13	<0.05	0.06	0.06	0.06	<0.05	<0.05	ND	<0.1	ND	ND
2, 3, 5-Trimethylnaphthalene	0.08	<0.05	<0.05	<0.05	<0.05	0.09	<0.05	ND	<0.1	ND	ND
Fluorene	0.11	<0.05	<0.05	<0.05	<0.05	0.10	<0.05	ND	<0.1	ND	ND
Phenanthrene	0.60	<0.05	0.12	0.07	0.11	0.52	0.08	ND	0.49	ND	ND
Anthracene	0.05	<0.05	<0.05	<0.05	<0.05	0.05	<0.05	ND	<0.1	ND	ND
1-Methylphenanthrene	<0.05	<0.05	<0.05	<0.05	<0.05	<0.05	<0.05	ND	<0.1	ND	ND
Fluoranthene	0.13	<0.05	<0.05	<0.05	<0.05	0.13	<0.05	ND	0.15	ND	ND
Pyrene	0.05	<0.05	<0.05	<0.05	<0.05	0.06	<0.05	ND	<0.1	ND	ND
Total concentrations of PAHs	3.08	0.42	1.36	0.78	1.02	2.43	1.24	ND	3.10	ND	ND
Micrograms of total PAHs (background subtracted) per gram of smoke			650		770	6400					

at the end of the burn. In contrast, two pool fires in Kuwait[24] produced CO/CO_2 ratios of 0.007 and 0.012. Again, this indicates a lower combustion efficiency (i.e., more oxygen starvation) for the NOBE burns than for the Kuwait pool fires. One reason for the difference may be that the two Kuwait pool fires discussed by Laursen et al.[24] contained venting wells in their centers, which probably released natural gas as well as crude oil.

CO concentrations were low and were difficult to quantify for many of the more dilute smoke samples. From measurements of the ratio of CO to excess CO_2, and from multiplying this ratio by the emission factor for CO_2, the emission factor for CO was estimated to be ~13 g kg^{-1}. The emission factor for SO_2 (~3 g of SO_2 per kg fuel) was determined by assuming all of the sulfur in the fuel (0.15%) was emitted in the smoke.

Based on our limited measurements of the emissions factors for VOCs (~5 g kg^{-1}), it appears that little unburned hydrocarbon vapor escaped the flame zone.

3.10 *Smoke Concentrations Derived from Lidar*

Derivation of smoke concentrations from lidar could not be carried out for the first burn because the low clouds present obscured the lidar return from the sea surface.

Figure 9 shows a sketch of the second NOBE burn, and the locations of the four cross-sectional measurements of the plume with the lidar. A lidar profile along the length of the plume was also obtained as the aircraft flew above the plume. The first three cross sections and the lengthwise section of the plume were obtained within minutes of each other, the fourth cross section was made about an hour later. The surface winds were southerly, but veered toward westerly with height.

Figure 10 shows the measured mean wind profile for the second NOBE burn. The initial rise of the smoke plume was variable, due to the fire pulsing varying sizes of smoke parcels. The smoke that started near the surface was advected almost due north, but smoke that rose higher was sheared off toward the east.

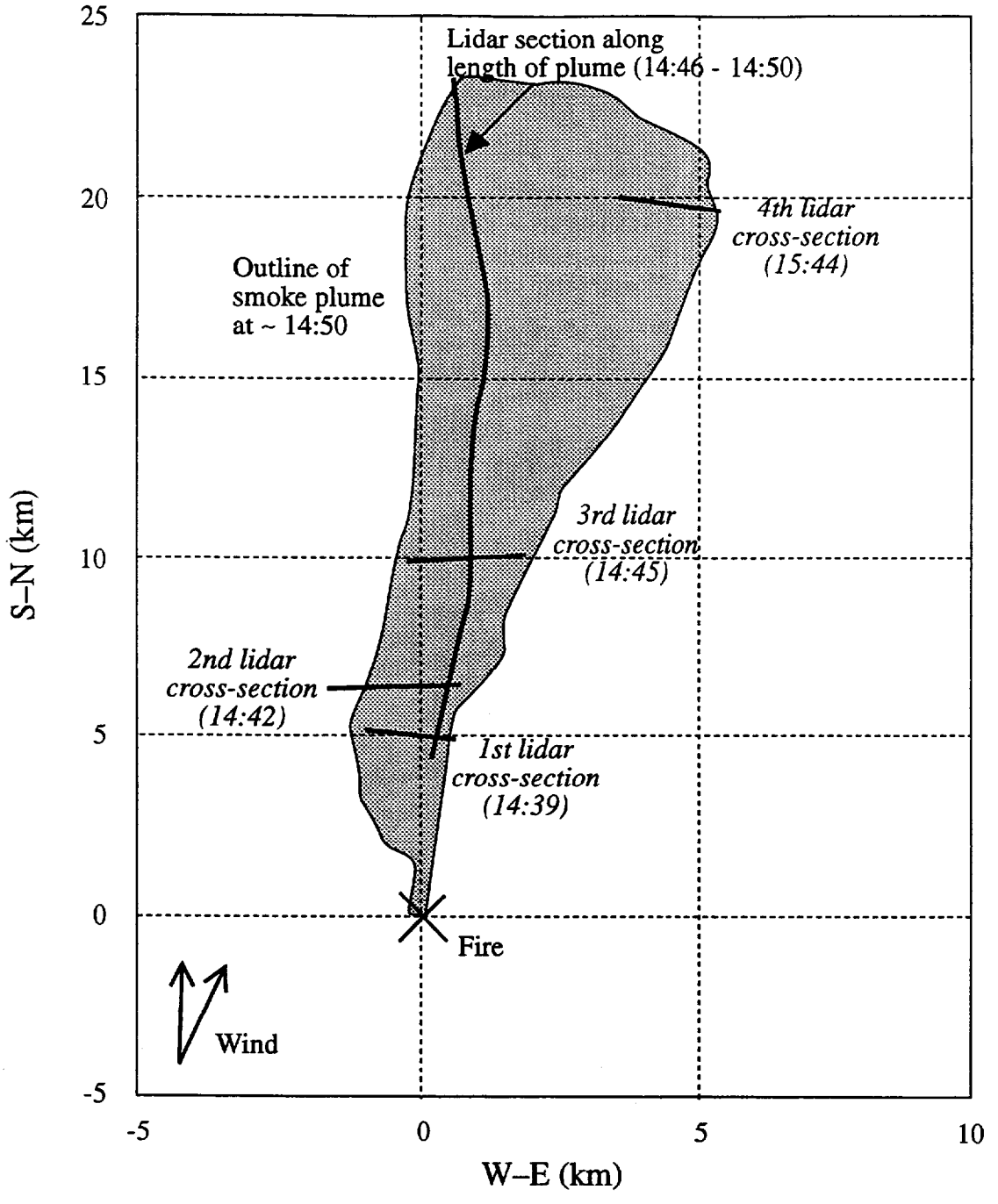

Figure 9. Schematic of the smoke plume from the second NOBE burn showing where the airborne lidar measurements were obtained.

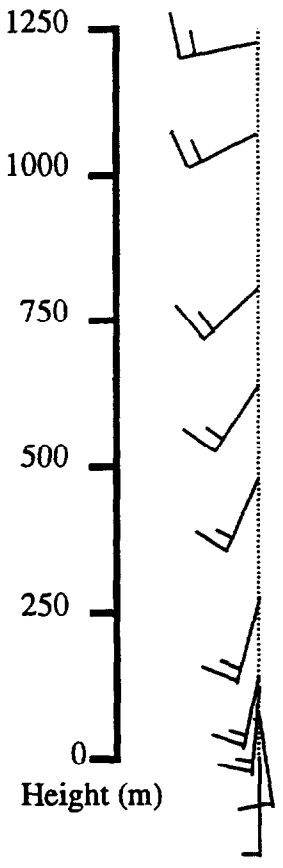

Figure 10. Vertical profile of mean winds during the second NOBE burn.

Figure 11 shows the mass concentrations of smoke particles derived from the four lidar cross sections of the smoke plume for the second NOBE burn. Also shown in each case are the derived optical depths (at $\lambda = 0.532$ μm) of the smoke.

Figures 11a and b show the results from the first and second lidar cross sections of the smoke plume, respectively. Some smoke was detected down to about 50 m from the ocean surface. This may have been due to either a smoke parcel that never rose very high to begin with or to fumigation. Both cross sections show the tilted, sheared structure of the plume near the fire. The peak mass concentrations of particles in the first two cross sections were just over 350 μg m^{-3}, with large portions of the plume containing particle concentrations between 150 and 250 μg m^{-3}. Considering their proximities to the burn, these concentrations are fairly low. This is also reflected in the small values of optical depth; even in the heaviest parts of the first two cross sections the optical depth was only about 0.2.

The third lidar cross section is shown in Figure 11c. Here, the plume is less organized, and consists of two separated regions of smoke. Also, the smoke concentrations are significantly higher than in the first two cross sections; peak values are > 550 μg m^{-3} and large areas of the plume have smoke concentrations > 250 μg m^{-3}. The optical depth across the plume is correspondingly higher. The higher mass concentrations of smoke in the third cross section are in spite of the fact that smoke in this region was ~8–12 minutes older than in the first two cross sections, and therefore had more time to diffuse. This variability reflects the fluctuating burn rate of the oil. Figure 11c shows that the smoke had risen to over 750 m above the surface at 10 km downwind. This was probably due, in part, to the fact that the fire was larger and more intense at the time this smoke was produced. However, the smoke may also have been lifted as it moved downwind due to heating from the absorption of solar radiation (see below).

The fourth lidar cross section (Figure 11d) was taken about 20 km downwind of the fire, at about an hour after the first three cross sections. The smoke was much more

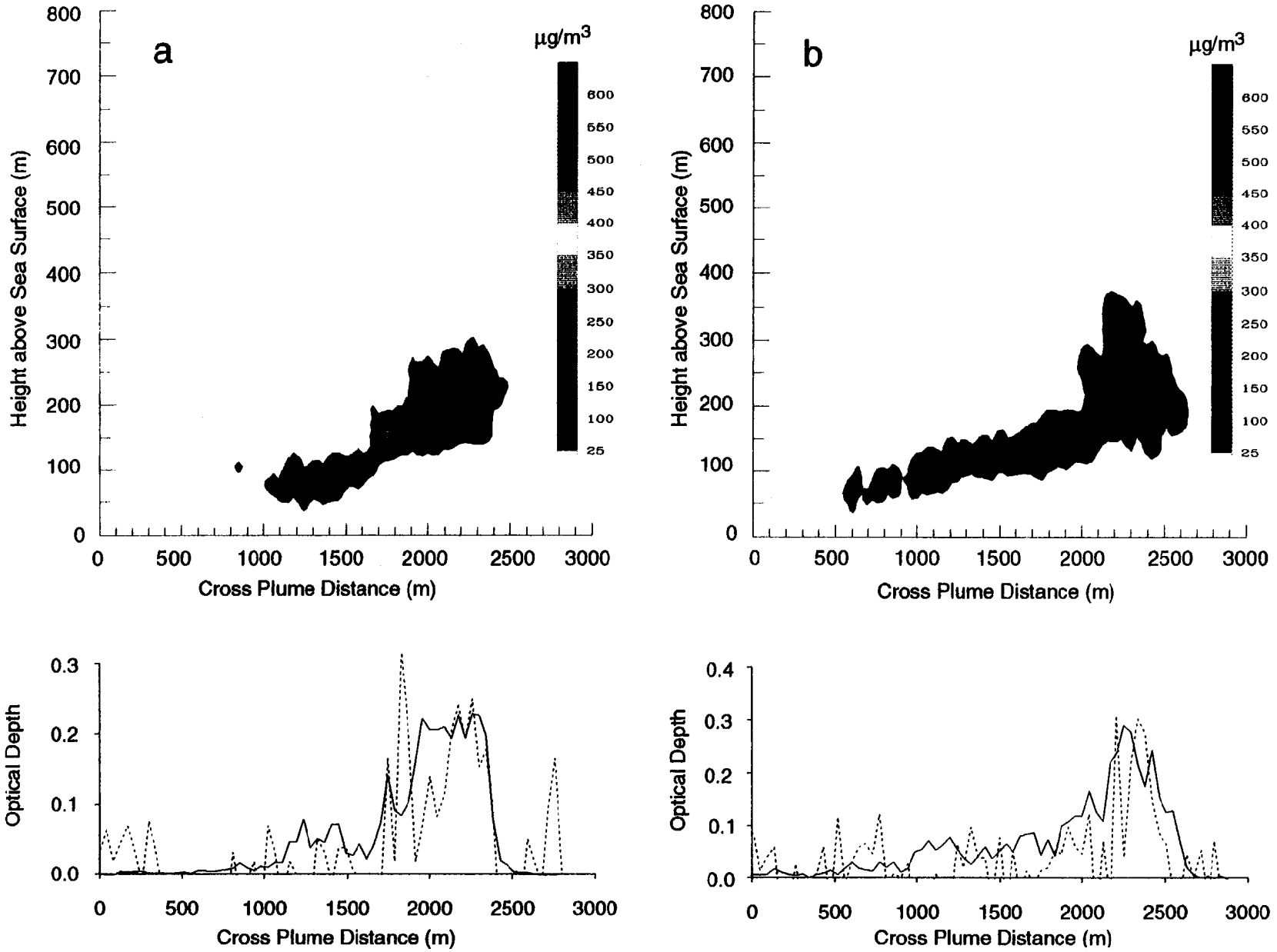

Figure 11. (a) Contours of mass concentrations of smoke particles for the second NOBE burn derived from the airborne lidar measurements for the first vertical cross section across the width of the smoke plume (see Figure 9). Also shown are the optical depths of the smoke derived from the lidar backscatter profile (solid line) and from the strength of the laser return from the ocean (dashed lines). (b) As for (a) but for the second vertical cross section shown in Figure 9. (c) As for (a) but for the third vertical cross section shown in Figure 9. (d) As for (a) but for the fourth vertical cross section shown in Figure 9. Note that the vertical scale for (d) is displaced by 200 m from that for (a)–(c).

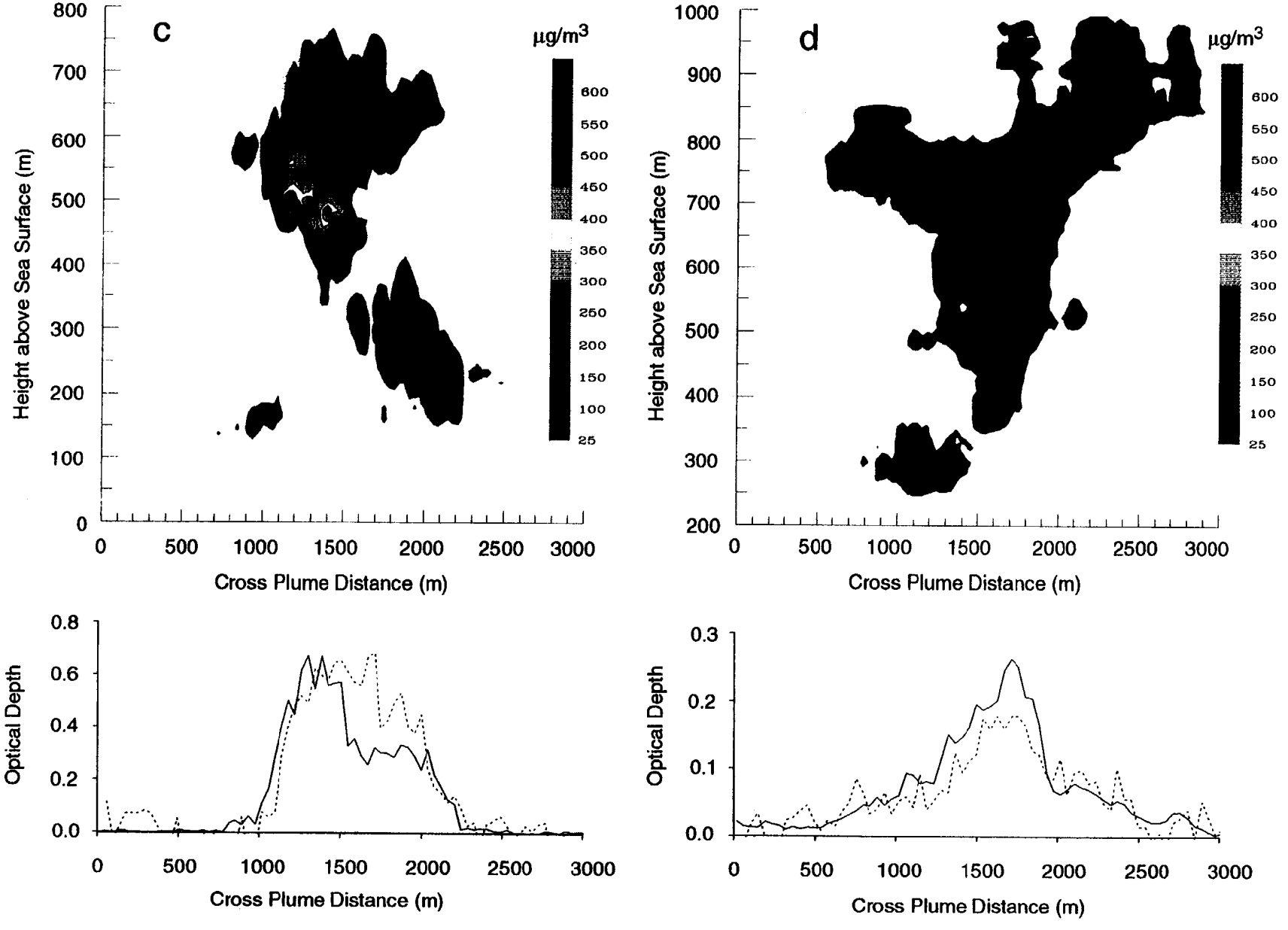

Figure 11. (continued)

diffuse in this cross section, with mass concentrations generally < 100 $\mu g\ m^{-3}$. Also, the smoke was at a higher altitude than in the first three cross sections. At this distance downwind, the optical depth across the plume was almost Gaussian in shape.

Figure 12 shows the mass concentrations of particles in the smoke, derived from the lidar measurements, as the aircraft flew along the length of the smoke plume. The highly variable shape of the plume is revealed in this figure; also, the top of the smoke plume is seen to be more irregular than the base, especially from 2 to 6 km downwind. Overall, the height of the plume gradually increased with distance downwind. Some of the internal structure of the plume is also revealed in Figure 12.

Particle concentrations in the plume did not decrease with increasing distance from the fire in any simple fashion; this is because of the variability in the burn rate of the oil and the very slow dispersion of the smoke. In fact, the peak particle concentration (> 800 $\mu g\ m^{-3}$) was located at ~8.5 km downwind (the color scale in Figure 12 was not extended to encompass this isolated spot because it would have caused a loss of resolution in depicting the rest of the plume), and a fairly dense parcel of smoke is seen at ~14 km downwind.

The optical depth of the plume was generally below 0.3, with only one region over 0.6. The very high optical depths (indicated by the dashed line at downwind distances < 1.5 km in Figure 12) are incorrect since they were measured as the aircraft was banking through a turn so that the laser beam was not pointing straight down. The solid lines in Figure 12 reflect more accurate values of the optical depth.

A word of caution is in order concerning the interpretation of the fine-scale details in Figures 11 and 12. The lidar signal contained some electronic and random noise. Some filtering was performed, but this was kept to a minimum so as not to eliminate real signals. The large-scale structure of the plume should be accurately represented in Figures 11 and 12, as should the magnitudes and gradients of the concentrations of particle concentrations in the plume. However, small details, such as the region of clear air just beyond 11 km or the flat top to the smoke plume at 9.5 km in Figure 12, could be erroneous.

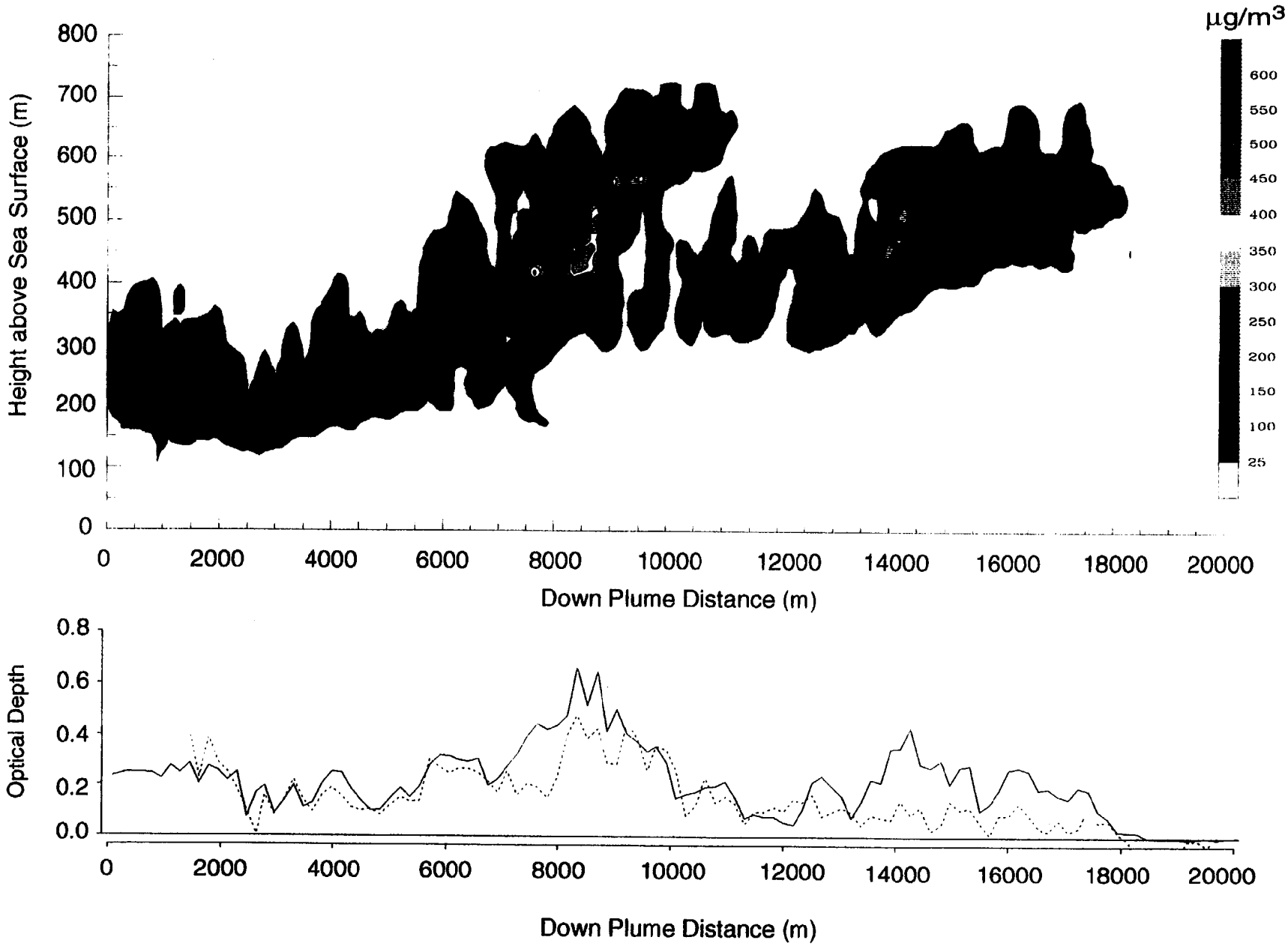

Figure 12. As for Figure 11 but for the vertical cross section along the length of the smoke plume.

3.11 *Mass Fluxes of Smoke*

The contours of the concentrations of particles in cross-sections of the smoke plume shown in Figure 11 can be integrated and combined with the wind speed to yield the mass fluxes of particles passing through each of the four cross sections. The fluxes derived this way for cross sections 1–4 were 142, 175, 423, and 414 g s^{-1}, respectively. In the second NOBE burn, 28.5 m^3 of oil burned in 1.3 hours[28], the density of the oil was 0.84 kg per liter, and the sub-3.5 μm diameter particle emission factor was 87 g kg^{-1}. These quantities can be combined to yield an average smoke mass flux from the second NOBE burn of ~447 g s^{-1}, which, considering the variability in the rate of burning, is in reasonable agreement with the findings derived from the lidar measurements at various distances (times) downwind.

3.12 *Self-lofting of Smoke due to Solar Heating*

Smoke particles of elemental carbon strongly absorb visible light. This warming tends to make the smoke rise; this is called *self-lofting*. We can make a rough estimate of the heating rate of the smoke as follows. The contour plots of the mass concentration of smoke particles (Figures 11 and 12) show that the average value was ~ 200 μg m^{-3}. Combining this with the measured values of the specific extinction of the smoke ($A_e = \sigma_{ext}/\rho_a = 8.7$ m^2 g^{-1}) and the single-scattering albedo ($\omega = 0.32$) yields an average absorption coefficient of ~$1.x10^{-3}$ m^{-1}. The flux of solar radiation was ~800 W m^{-2}. This, combined with the absorption coefficient and the specific heat per unit volume for air (c_p ~1250 J $°C^{-1}$ m^{-3}), yields a heating rate for the smoke of ~2.5 °C h^{-1}.

The rates of rise of portions of the smoke are consistent with this heating rate. For example, the smoke shown in Figure 12 is at a height of ~400 m at ~10 km downwind, and at 17.5 km downwind it is at a height of ~550 m. The time taken for a smoke parcel to travel this distance at the measured wind speed would have been ~1000 s. If heated at 2.5 °C h^{-1}, the predicted increase in the height of the smoke in 1000 s, in the stable ambient

atmosphere that characterized the NOBE burns, is ~140 m, compared to the observed value of ~150 m.

4. DISCUSSION

To put the NOBE burns into perspective with other large-scale combustion sources, we have used our measured emission factors and the approximate burn rates for NOBE and calculated the total emission rates (in kg hr^{-1}) for the major combustion products. The results are summarized in Table 5.

We see from Table 5 that for CO_2 the hourly emission rate from the NOBE was equivalent to approximately 2 acres of slash burning (typical slash burns are on the order of several tens to several hundreds of acres). For CO the equivalent amount of slash burning is much smaller (0.2 acres), since slash burns have a high degree of smoldering combustion that promotes CO formation. For SO_2 the emissions are proportional to the sulfur content of the crude oil, which was quite low in the NOBE burn (0.15%); this resulted in an emission rate of SO_2 that was much lower than that from a typical coal-fired electric power generating plant. The total particle emission rate for the NOBE burns (4050 kg hr^{-1}) was calculated from a total particle emission factor of 150 g kg^{-1} derived from filter measurements aboard the NIST blimp. A smoke sample collected with a cascade impactor aboard the blimp showed that ~65% of the total mass was in particles <3.5 μm diameter. Therefore, based on these measurements, the emission factor for particles <3.5 μm diameter should have been 150 x 0.65 = 98 g kg^{-1}. This agrees well with our measured emissions factor for particles <3.5 μm diameter, of 87 ± 15 g kg^{-1}. A total particle emission rate of 4050 kg hr^{-1} is comparable to the smoke emitted from ~9 acres of slash burning, or about 58,000 wood stoves (an efficiently burning wood stove produces relatively little smoke per kilogram of fuel burned). Emissions of sub-3.5 μm diameter smoke particles from the NOBE burns were equal to ~7 acres of slash burning, and, if we subdivide this into elemental (soot) and organic carbon fractions, similar comparisons can

TABLE 5. Calculated Rates of Emission* for the NOBE Burns (With an Average Burn Rate of 200 Barrels of Oil per Hour or 27,000 kg hr^{-1})

	Emission Factor ($g\ kg^{-1}$)	Emission Rate ($kg\ hr^{-1}$)	Comparable Emissions from Other Sources
CO_2	2810	75900	~ 2-acre slash burn[31]
CO	30	810	~ 0.2-acre slash burn[31] or ~ 2,400 woodstoves[32]
SO_2	3	81	7400 kg hr^{-1} (average coal-fired powerplant)[33]
Total smoke particles[30]	150	4050	~ 9-acre slash burn[31] or ~ 58,000 woodstoves[32]
Sub-3.5 μm diameter smoke particles	87	2350	~ 7-acre slash burn[31]
Sub-3.5 μm diameter soot (elemental carbon)	66	1782	~ 46-acre slash burn[34,35]
Sub-3.5 μm diameter organic carbon aerosol	7	186	~ 99 kg hr^{-1} (emissions from cigarette smoke in Los Angeles area)[36] or ~ 4,300 woodstoves[32]
VOC	5	132	Equivalent to natural emissions from a living 9,000-acre forest[37] or ~ 1,000 woodstoves[32]
PAHs**	~ 0.1	~ 2.7	Equivalent to ~ 4,400 woodstoves[32] or ~ 17 acre slash burn[31]

* In this table we define the emission factor as the total mass of the chemical species emitted per unit mass of fuel burned.

** Approximate upper limit; samples were only slightly greater than blanks.

be made to other sources of these materials (Table 5). The emissions of VOCs from NOBE were quite small, since little unburned fuel escaped the flame zone of a pool fire.

In the case of PAHs, all of the airborne samples collected in the smoke plume from NOBE were at or near the detection limit. We therefore chose an approximate upper limit to our measurements and derived an approximate maximum value for the emission rate of PAHs (see Table 5). An accurate emission rate for PAH will have to be determined from the PAH-to-mass ratio measured by Environment Canada near the fire, where detectable amounts of PAH were measured.

The above comparisons should be useful in placing the emissions from the NOBE oil burns in perspective with other sources of air pollution.

5. CONCLUSIONS

The smoke from the two NOBE burns contained high concentrations of submicron, respirable particles. Number concentrations in the accumulation mode were up to 4,000 cm^{-3} out to 30 km from the fire. Mass loadings near 100 $\mu g\ m^{-3}$ were measured out to 25 km at plume level. However, these high particulate concentrations were not measured at sea level, since the smoke plume rose quickly to the upper part of the boundary layer (~300–500 m MSL), and some smoke penetrated higher as the fire pulsed larger buoyant parcels. The stable atmospheric conditions under which the NOBE burns occurred inhibited any smoke from mixing back down to the surface. This was confirmed by an aircraft pass beneath the plume at ~24 km downwind in which smoke near the surface was not detected. In general, the intensity of a fire and the stability of the lower atmosphere will determine whether (and in what amounts) smoke will intercept the surface.

The average sub-3.5 μm diameter particle emission factor from the NOBE burns was $87\pm15\ g\ kg^{-1}$, which agrees well with a cascade impactor measurement obtained aboard the NIST blimp. The composition of the smoke particles, on average, was 76% elemental carbon, 8% organic carbon and 16% unidentified materials.

Polycyclic aromatic hydrocarbon concentrations in the smoke plume were similar to those measured in background samples near the ships, and lower than those measured on two out of the five control blanks. Two samples of the smoke produced quite low PAH concentrations of 650 and 770 (μg PAH g^{-1} smoke) but a third (possibly contaminated with ship exhaust) had a concentration of 6400 (μg PAH g^{-1} smoke). These results are therefore highly uncertain.

This study confirms that *in situ* burning is an effective method of removing spilled oil from the ocean and that, under appropriate conditions, the effects on air quality at the surface are negligible. Most of the oil was consumed and converted to benign products (e.g., CO_2 and H_2O), and the remaining pollutants were widely dispersed above sea level. Total amounts of pollutants released are comparable to or lower than a number of more familiar sources of pollution. However, if such a smoke plume remained on the surface, and was advected into a populated area, the impacts would probably be unacceptable due to the high particle concentrations.

Acknowledgments. We thank the crew of the C–131A for their help in collecting data. This study was supported by Environment Canada and the Alaska Department of Environmental Conservation.

REFERENCES

1. C. H. Thompson, G. W. Dawson, and J. L. Goodier, *Combustion: An Oil Spill Mitigation Tool*, U.S. Department of Energy DOE/EV-1830-1, National Technical Information Service, Springfield, VA 22161, 1979.
2. M. Fingas, and N. Larouche, "An introduction to in-situ burning of oil spills" *Envir. Canada, Spill Tech. Newsletter*, **15**, 4, (1990)

3. A. A. Allen, and R. J. Ferek, "Advantages and disadvantages of burning spilled oil" *Proceedings of the 1993 International Oil Spill Conference*, American Petroleum Institute, Washington, DC, 1993, pp. 765-772

4. J. Santodonato, P. Howard, and D. Basu, "Health and ecological assessment of polynuclear aromatic hydrocarbons", *J. Envir. Pathology and Toxicology*, **5**, 1, 1, (1981)

5. S. K. Yang, and B. D. Silverman, *Polycyclic Aromatic Hydrocarbon Carcinogenisis: Structure-activity Relationships*, CRC Press, Boca Raton, Florida, 1988

6. B. A. Benner Jr., N. P. Byner, S. A. Wise, G. W. Mulholland, R. C. Lao, and M. F. Fingas, "Polycyclic aromatic hydrocarbon emissions from the combustion of crude oil on water", *Envir. Sci. and Tech.*, **24**, 9, 1418, (1990)

7. P. V. Hobbs, H. Harrison, and E. Robinson, "Atmospheric effects of pollutants", *Science*, **183**, 4128, 909, (1974)

8. S. Twomey, "The influence of pollution on the shortwave albedo of clouds", *J. Atmos. Sci.*, **34**, 1149, (1974)

9. C. F. Rodgers, J. G. Hudson, B. Zielinska, R. L. Tanner, J. Hallett and J. G. Watson, "Cloud Condensation Nuclei from Biomass Burning", *Global Biomass Burning*, J. S. Levine, ed., The MIT Press, Cambridge, Mass., 1991, pp. 431 -438

10. G. Fiocco, and L. D. Smullin, "Detection of scattering layers in the upper atmosphere (60–140 km) by optical radar", *Nature*, **199**, 1275, (1963)

11. P. M. Hamilton, "The use of lidar in air pollution studies", *Int. J. Air Water Pollut.*, **10**, 427, (1966)

12. E. W. Barrett, and O. Ben-Dov, "Applications of lidar to air pollution measurements", *J. Appl. Meteor.*, **6**, 500 (1967)

13. W. B. Johnson, and E. E. Uthe, "Lidar study of the Keystone stack plume", *Atmos. Envir.*, **5**, 703, (1971)

14. L. F. Radke, C. A. Brock, J. H. Lyons, R. C. Schnell, and P. V. Hobbs, "Aerosol and lidar measurements of hazes in mid-latitude and polar airmasses", *Atmos. Envir.*, **23**, 2417, (1989)

15. R. M. Banta, L. D. Olivier, E. T. Holloway, R. A. Kropfli, B. W. Bartram, R. E. Cupp, and M. J. Post, "Smoke-column observations form two forest fires using doppler lidar and doppler radar", *J. Appl. Meteor.*, **31**, 1328, (1992)

16. L. F. Radke, J. H. Lyons, and P. V. Hobbs, "Smokes from the burning of aviation fuel and their self-lofting by solar heating", *J. Geophys. Res.*, **95**, D9, 14,071 (1990)

17. L. F. Radke, D. A. Hegg, J. H. Lyons, C. A. Brock, P. V. Hobbs, R. Weiss, and R. Rasmussen, "Airborne measurements of smokes from biomass burning", *Aerosols and Climate*, A. Deepak Publishing, Hampton, Virginia, 1988, pp. 411–422

18. R. E. Weiss, and P. V. Hobbs, "Optical extinction properties of smoke from the Kuwait oil fires", *J. Geophys. Res.*, **97**, D13, 14,537 (1992)

19. J. J. Huntzicker, R. L. Johnson, J. J. Shah, and R. A. Cary, "Analysis of organic and elemental carbon in ambient aerosols by a thermal-optical method", *Particulate Carbon: Atmospheric Life Cycle: Atmospheric Life Cycle*, Plenum Press, New York, 1982, pp. 79–88

20. A. P. Waggoner, N. C. Ahlquist, and R. J. Charlson, "Measurement of the aerosol total scatter-backscatter ratio", *Appli. Optics*, **11**, 2886 (1972)

21. G. A. d'Ameida, P. Koepke, and E. P. Shettle, *Atmospheric Aerosols: Global Climatology and Radiative Characteristics*, Deepak Pub., Hampton, Virginia, 1991, pp. 237.

22. C. M. R. Platt, "Remote sounding of high clouds: I. Calculations of visible and infrared optical properties from lidar and radiometer measurements", *J Appl. Meteor.*, **18**, 1130 (1979)

23. J. S. Reid, T. A. Cahill and P. H. Wakabayashi, "Geometric/aerodynamic equivalent diameter ratios of ash aggregate aerosols collected in burning Kuwaiti well fields", *Atmos. Environ.*, **28**, 2227 (1994)

24. K. K. Laursen, R. J. Ferek, and P. V. Hobbs, "Emission factors for particles, elemental carbon, and trace gases from the Kuwait oil fires", *J. Geophys. Res.*, **97**, D13, 14,491 (1992)

25. H. Koseki, and G. W. Mulholland, "The effect of diameter on the burning of crude oil pool fires", *Fire Tech.*, **54** (1991)

26. C. W. Bruce, T. F. Stromberg, K. P. Gurton, and J. B. Mozer, "Trans-spectral absorption and scattering of electromagnetic radiation by diesel soot", *Appl. Optics*, **30**, 1,537 (1991)

27. D. M. Roessler, and F. R. Faxvog, "Optical properties of agglomerated acetylene smoke particles at 0.5145 μm and 10.6 μm wavelengths", *J. Opt. Soc. Amer.*, **70**, 230 (1980)

28. M. F. Fingas, F. Ackerman, K. Li, P. Lambert, Z. Wang, M. C. Bissonnette, P. R. Campagna, P. Boileau, N. Laroche, P. Jokuty, R. Nelson, R. D. Turpin, M. J. Trespalacios, G. Halley, J. Belanger, J. Paré, N. Vanderkooy, E. J. Tennyson, D. Aurand, and R. Hiltabrand, "The Newfoundland Offshore Burn Experiment-NOBE, preliminary results of emissions measurement," in *Proceedings of the 17th Arctic and Marine Oilspill Program (AMOP) Technical Seminal*, Vancouver, BC, June 8–10, 1994, pp. 1099–1163

29. NRC (National Research Council), *Human Exposure Assessment for Airborne Pollutants, Advances and Opportunities*, National Academy Press, Washington D. C., 1991, pg. 221

30. W. D. Walton, W. H. Twilley, J. McElroy, D. D. Evans and E. J. Tennyson, "Smoke measurements using a tethered miniblimp at the Newfoundland Offshore

Burn Experiment", *Proceedings of the 17th Arctic and Marine Oilspill Program (AMOP) Technical Seminar*, Vancouver, BC, June 8–10, 1994, pp. 1083-1098

31. J. Peterson, and D. E. Ward, "An inventory of particulate matter and air toxics emissions from prescribed fires in the United States for 1989." *Final report for 1989*, USDA Forest Service, Pacific Northwest Research Station, Seattle, Washington, 1993, pp. 50–54
32. T. V. Larson, and J. Q. Koenig, "Woodsmoke: Emissions and non-cancerous respiratory effects", *Annv. Rev. Public Health*, **15**, 1994, pp. 133–156
33. D. A. Hegg, and P. V. Hobbs, "Measurements of gas-to-particle conversion in the plumes from five coal-fired electric power plants", *Atmos. Environ.*, **14**, pp. 99–116, 1980
34. R. A. Susott, D. E. Ward, R. E. Babbitt, and D. J. Latham, "The measurement of trace emissions and combustion characteristics for a mass fire", *Global Biomass Burning*, J. S. Levine ed., The MIT Press, Cambridge, Mass., 1991, pp. 245–257
35. W. Einfeld, D. E. Ward, and C. C. Hardy, "Effects of fire behavior on prescribed fire smoke characteristics: A case study", *Global Biomass Burning*, J. S. Levine ed., The MIT Press, Cambridge, Mass., 1991, pp. 412–419
36. G. R. Cass, P. M. Boone, and E. S. Macias, "Emissions and air quality relationships for atmospheric carbon particles in Los Angeles", *Particulate Carbon: Atmospheric Life Cycle*, G. T. Wolfe ad R. L. Klimisch, eds., Plenum Press, New York, 1982, pp. 207–240
37. S. A. McKeen, E.-Y. Hsie, and S. C. Liu, "A study of the dependence of rural ozone on ozone precursors in the eastern United States", *J. Geophys. Res.*, **96**, 1991, pp. 15377–15349